Knowledge-Based Systems 318 (2025) 113527

Contents lists available at ScienceDirect

Knowledge-Based Systems

journal homepage: www.elsevier.com/locate/knosys

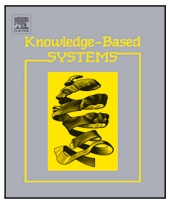

Multidimensional robustness analysis for optimizing complex systems

João Ricardo B. Paiva [a,e], Viviane M. Gomes Pacheco [a,c,e], Júnio Santos Bulhões [a,d,e], Clóves Gonçalves Rodrigues [c], António Paulo Coimbra [b], Wesley Pacheco Calixto [a,b,e,*]

[a] Electrical, Mechanical & Computer Engineering School, Federal University of Goias, Goiania, 74605-220, Goias, Brazil
[b] Institute of Systems and Robotics (ISR), Coimbra University, Coimbra, 3030-290, Portugal
[c] Polytechnic and Arts School, Pontifical Catholic University of Goias, Goiania, 74605-010, Brazil
[d] Federal Institute of Mato Grosso, Primavera do Leste, 78850-000, Brazil
[e] Technology Research and Development Center (GCITE), Federal Institute of Goias, Goiania, 74055-110, Goias, Brazil

ARTICLE INFO

Keywords:
Operational robustness
System performance
System complexity
System stability
Multidimensional analysis

ABSTRACT

This work proposes the development of a metric for the analysis of operational robustness in systems, focusing on performance, complexity, and stability as key components. The methodology integrates these factors, enabling the assessment of the system's ability to meet its design requirements, its internal dynamics and external interactions, and its capacity to return to equilibrium after disturbances. The metric is applied in three case studies: an intensive care unit, process scheduling in operating systems, and traction and braking in electric vehicles. The results show that, in scenarios with higher robustness, the contributions of performance, complexity and stability are balanced, with performance contributing around 30% and complexity and stability each contributing approximately 35%. In contrast, scenarios with lower robustness exhibit greater variation in the contributions of these components. These findings suggest that the proposed metric is an efficient tool for both quantitative and qualitative analyses, providing more detailed perspectives for decision making in complex systems.

1. Introduction

System analysis is often conducted with an exclusive focus on performance, a practice considered limiting. Ilgen and Schneider [1] emphasize the importance of a multidisciplinary approach in evaluating system performance. Borman & Brush [2] suggest evaluating the overall performance of the system through a multidimensional analysis, taking into account the performance of different components of the system. This perspective suggests that the overall performance is the aggregation of the performance of specific segments of the system [3]. Campbell [4] highlights the need to use performance metrics that reflect compliance with established requirements, allowing an accurate evaluation of the efficiency of the system. Cadwell [5] demonstrates that system performance can fluctuate throughout its operation, even in the most established systems. The complexity and other dynamics of the system must be analyzed, as described by Simon [6], who argues that general properties cannot be easily deduced solely from analyzing parts and their interactions. Bak & Wiesenfeld [7] attribute significant complexity in systems to self-organization, highlighting the ability of these systems to autonomously modify their behavior and structure over time.

The complexity of systems emerges from the varied and unpredictable interactions among their elements, as Simon [8], leading to multiple levels of complexity. The definition of complexity lacks consensus, with Sussman [9] presenting twenty different definitions, and Lloyd [10] proposing a classification based on the difficulty of description and the level of organization. The increase in regulations within human organizations adds layers of complexity to the study of complex systems [11–13]. Holland [14] and Mitchell [15] argue that the absence of a universal definition does not hinder the study of these systems, offering approaches to address their emergent nature. Mobus et al. [16] emphasize the need for a systemic organization to determine complexity. To quantify this complexity, a variety of metrics are used, including entropy, statistical analyses, fractal dimension, algorithmic information content, dynamic depth, and system connectivity [17–28], significantly enriching the analysis and understanding of complex systems.

Paice & Wirth [29] argue that self-regulation mechanisms ensure the stability of complex systems in the face of unforeseen situations. Okuyama's methodology [30], which employs graph theory, is an effective tool for assessing stability. Pesterev [31] introduces the concept of stability sectors in control systems, and the studies by Chestnov

* Corresponding author at: Electrical, Mechanical & Computer Engineering School, Federal University of Goias, Goiania, 74605-220, Goias, Brazil.
E-mail address: wesley.pacheco@ufg.br (W.P. Calixto).

https://doi.org/10.1016/j.knosys.2025.113527
Received 23 October 2024; Received in revised form 21 March 2025; Accepted 7 April 2025
Available online 16 April 2025
0950-7051/© 2025 The Authors. Published by Elsevier B.V. This is an open access article under the CC BY-NC license (http://creativecommons.org/licenses/by-nc/4.0/).

and Shatov [32] and Liu et al. [33] demonstrate how stability varies under different operating conditions and loads. The research by Zhong et al. [34] and Wan & Luo [35] explores the interconnections between performance, complexity, stability and optimization, suggesting methods to optimize problem solving and system modeling. Laddha and Ramalingam [36] and Hammami [37] discuss the importance of adapting optimization processes to the specific characteristics of the systems, considering the heterogeneity of the components.

Advanced optimization techniques are used to define parameters that ensure the adaptability of the system to unexpected situations while maintaining functional stability [38,39]. Keshtkar et al. [40] propose a methodology that integrates concepts of stability and optimization in mechanical contexts. In the specific fields of power systems and wind energy, Odintsov et al. [41] and Nassar et al. [42] investigate the incorporation of stability into optimization procedures to achieve solutions that balance stability with compliance with required system standards. Research in this area is expanding, addressing uncertainties in performance evaluation methods, discrepancies in the conceptualization of complexity, the importance of considering stability alongside performance and complexity in specific operational contexts, and the need to adapt optimization processes to include these critical dimensions [43].

Although recent advances represent important contributions, current methodologies still exhibit significant limitations in addressing the interaction between performance, complexity, and stability. Existing approaches typically assess these aspects in isolation, resulting in partial or inconsistent analyses [44]. Performance metrics tend to focus primarily on efficiency and compliance with predefined requirements [1,2], often neglecting the systemic effects of complexity and stability. However, even fully optimized systems can show unpredictable behavior due to emergent properties and non-linear interactions among components [7,8].

Quantifying complexity remains a challenge due to the large number of definitions and evaluation criteria [9,10]. Although some methodologies consider structural and organizational aspects [14,15], others focus on statistical and algorithmic measures [16]. Similarly, stability is often assessed in isolation, without considering its dependence on both the complexity of the system and the operational conditions [31,33]. These fragmented perspectives hinder the development of comprehensive analyses and limit decision-making processes in complex systems.

To overcome these limitations, this study proposes an innovative metric that integrates performance, complexity, and stability into a unified framework. By jointly considering these three aspects, the proposed approach enables a more comprehensive assessment of system resilience, supporting more balanced and reliable optimization strategies. This integration is particularly relevant for the development of systems capable of maintaining operational consistency under varying conditions, ensuring both adaptability and resilience in real-world applications.

Thus, a gap is identified in current system analysis methods, characterized by the absence of a unified measure that simultaneously encompasses the concepts of performance, complexity and stability [45]. This study proposes the development of an integrated robustness metric capable of efficiently exploring the search space of input variables while accounting for the interaction among these three elements. The central hypothesis is that, if performance, complexity, and stability can be consistently measured in validated models, it becomes feasible to construct a metric that combines these dimensions and supports the identification of robust solutions.[1]

[1] In this work, system robustness refers to the ability of a system to continue operating correctly under adverse or unexpected conditions. Characteristics include resilience to faults, tolerance to disturbances, consistent performance, and adaptability [46,47].

The originality of the proposed approach lies in the integration of these three components into a single criterion, as well as in the introduction of specific methodologies for calculating the stability index. This approach differs from previous ones by enabling a more balanced and multidimensional evaluation of system robustness, overcoming the limitations of conventional metrics. The proposed method can be applied during both the design phase and in the operation of the system, with the potential to support decision making in various domains, such as engineering, computer science, economics, finance, and healthcare, especially in scenarios where adaptability is a key factor for sustained performance.

This study is organized as: Section 2 is dedicated to the theoretical foundation, presenting concepts such as systems, models, and optimization processes, which are required to understand the adopted methodology and the analysis of results. Section 3 details the proposed methodology, covering the entire process from model construction to results acquisition. Section 4 discusses the results obtained, while Section 5 concludes the study.

2. Theoretical background

This section presents the theoretical foundations that support the methodological proposal of the study. The chapter discusses the metrics commonly used in system analysis: performance, complexity, stability, and robustness, as well as their conceptual and operational limitations. The section also includes reflections on the nature of complex systems and the challenges associated with evaluating their properties in practical contexts.

2.1. Nature of the problem and sensitivity analysis of the parameters

Stacey [48] proposes classifying problems as simple, complicated, complex, or chaotic based on the level of disagreement and uncertainty about the problem and the uncertainty regarding the methods to address it. Simple problems are well understood and have known solutions, while chaotic problems are characterized by a lack of agreement and the absence of known methods for resolving them. The relationship between complexity, uncertainty, and resolution methods indicates that as the complexity and uncertainty of a problem increase, the choice of an appropriate method becomes more critical [49]. Fig. 1(a) illustrates these concepts using the Stacey matrix, which organizes problems according to the levels of disagreement and uncertainty. Meanwhile, Fig. 1(b) shows the relationship between complexity and uncertainty. Fig. 1(c), adapted from Paiva et al. [49], combines these concepts, showing how optimization methods can be applied to different regions of the matrix, depending on the nature of the problem.

In Fig. 1(c), deterministic methods are suitable for simple problems, while more unpredictable problems require sophisticated methods. For complicated issues, various methods can be used, such as deterministic, heuristic, and inferential approaches, depending on the level of uncertainty. Complex problems require heuristic, stochastic, or inferential approaches, whereas chaotic problems necessitate stochastic methods. Gomes [28] notes that uncertainty in systems emerges from variations in input parameters due to environmental changes that impact the output. Experiments with different parameter configurations allow the evaluation of performance under various circumstances, enabling sensitivity analyses to better understand the system behavior.

Sensitivity analysis is a technique that evaluates the impact of each input parameter on variations in the system's output [50,51]. According to Homma and Saltelli [52], this analysis quantifies the contribution of each input to the output of the real system or model. It is necessary for several purposes: (i) identifying the need for model simplification, (ii) investigating errors, (iii) assessing the system's sensitivity to variations, (iv) confirming the correct processing of input parameters, (v) reducing computational effort by converting irrelevant

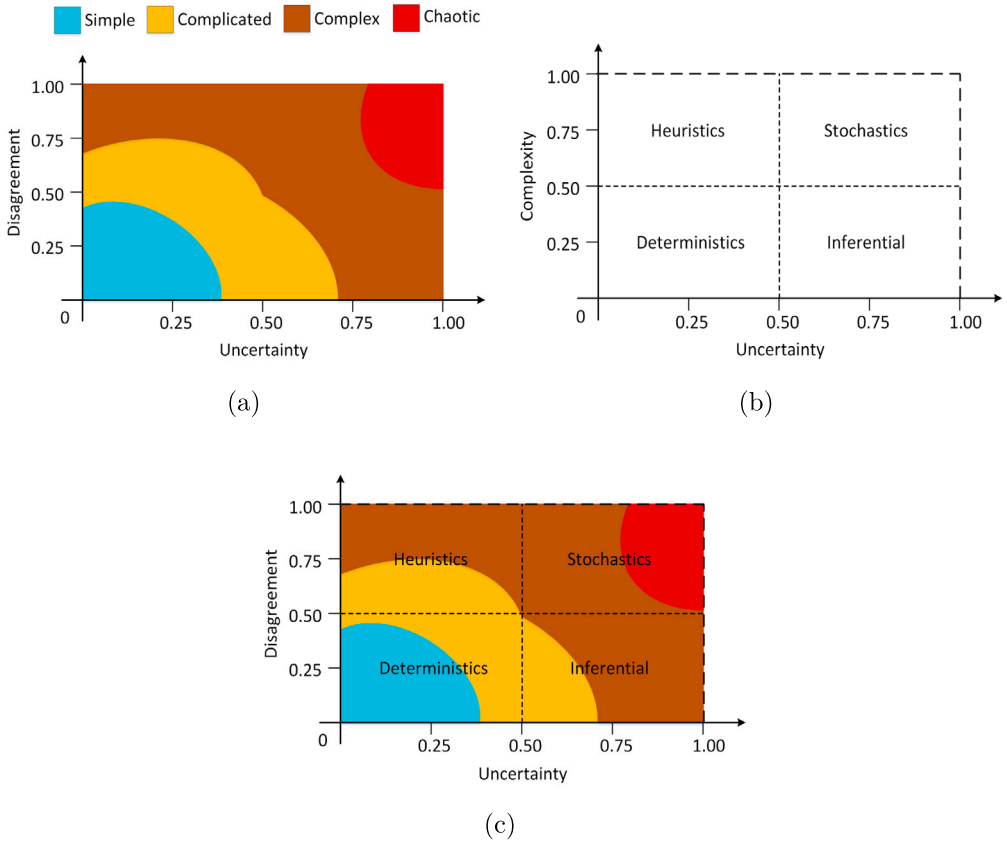

Fig. 1. Relationship between uncertainty, complexity, and disagreement: (a) Stacey Matrix, (b) optimization concepts, and (c) overlap of Stacey Matrix with optimization concepts.

input variables into constants, and (vi) identifying areas of interest in terms of system complexity and stability [51,53,54].

Sensitivity analysis can be local or global, depending on how the input parameters are varied. Local analysis alters one parameter at a time while keeping the others fixed at reference values, whereas global analysis considers the integrated variations of all input parameters [55,56]. Studies such as those by Hamby [57] and Frey and Patil [54] present various techniques for sensitivity analysis, comparing ten methods, including four analytical, five statistical, and one graphical approach. Saltelli et al. [51] provide a review of sensitivity analysis methods, with a focus on scientific models. This analysis is able to examine both the structure and dynamics of the system [58–60]. Among visual methods, Eschenbach and McKeague [61] propose the use of the spider diagram.

Fig. 2, adapted from Gomes et al. [28], presents the spider diagram for the sensitivity analysis of a system with two parameters, which can be generalized to n input parameters $x_1, x_2, \ldots, x_i, \ldots, x_n$. In local sensitivity analysis, the reference values that optimize system performance, known as the baseline case $\vec{\beta}$, are identified by (1). In the spider diagram, the vertical axis represents the system outputs, while the horizontal axis indicates the variation of parameters relative to the reference value. The blue and red curves represent the simulation results for parameters x_1 and x_2, allowing for the evaluation of the sensitivity of each parameter based on the distance of the curves from the baseline axis.

$$\vec{\beta} = [x_1^{\beta}, x_2^{\beta}, \ldots, x_i^{\beta}, \ldots, x_n^{\beta}] \tag{1}$$

During each cycle of the analysis, one parameter is varied while the others remain constant at their reference values. This creates new scenarios by combining different values of the parameter under analysis with the reference values of the other parameters. These scenarios are then applied to the real or simulated system and the corresponding outputs are recorded, allowing for the evaluation of the sensitivity of each parameter x_i. In Fig. 2, the analysis range varies from $[-80\%, 60\%]$, with parameters adjusted within the interval $[-100\%, 100\%]$ from their reference values. However, in practical applications, certain parameters may be subject to physical or strategic limitations that restrict this range. Even with such restrictions, a parameter may still be highly sensitive, with its variation exerting a significant impact on the system's output.

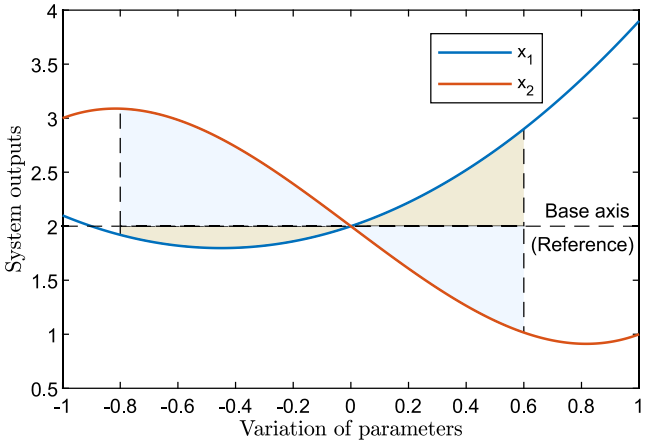

Fig. 2. Spider diagram for a system with two input parameters.

Gomes et al. [28] propose the area method for determining the sensitivity indices of the input parameters of the system. In this method, the contribution of each parameter is evaluated on the basis of the area formed between its curve and the baseline axis, which represents the system's output in the baseline case. In Fig. 2, the contributions of the parameters x_1 and x_2 are highlighted in blue and brown, respectively.

The sensitivity index of parameter x_i is calculated using (2), where $S^a_{x_i}$ is the sensitivity index, A_{x_i} is the area under the curve of parameter x_i, and n is the total number of input parameters [28].

$$S^a_{x_i} = \frac{A_{x_i}}{\sum_{i=1}^{n} A_{x_i}} \tag{2}$$

2.2. Measures of performance, complexity, stability, and robustness

Ilgen and Schneider [1] and Borman and Brush [2] state that performance reflects the degree to which a system meets imposed constraints in multiple aspects considered in the analysis. In essence, system performance results from the interaction between the performance of each system component that performs specific functions [3]. Therefore, performance metrics should provide quantitative values that allow comparisons between different system operation scenarios [4]. According to Fetsch and DeBasio [62], performance refers to the extent to which the system's objectives are achieved. High performance is achieved when the system operates optimally using available resources, yielding satisfactory values for performance metrics [63,64]. To develop a system performance metric, it is necessary to integrate relevant information on the aspects considered significant by analysts.

Complexity emerges from interactions between parts, leading to unpredictable behavior [14]. Page [65] suggests combining techniques from different fields to address complex problems due to the variety of approaches available. Even simple systems can exhibit complexity due to the multitude of interactions [66]. In addition to the unifying characteristics proposed by the science of systems, complex systems display non-linearity, emergence, self-organization, diversity, and interdependence [66–68]. These characteristics are analyzed to determine the level of complexity [28]. Emergence results from simple rules that generate complex behavior [15]. Self-organization is derived from the ability of parts to adjust their operations [65,69,70]. Diversity allows each part to contribute uniquely [65,71]. The interdependence shows how the removal of parts affects the whole [11]. Complexity metrics evaluate these and other characteristics [15,72]. Mitchell [15] indicates that these metrics are useful for comparing different systems. Gomes et al. [28] propose the natural complexity metric, which assesses the importance of connections. This metric considers interactions between entities, resources, and queues, calculating the complexity of the system during simulation.

In the natural complexity metric, interactions are recorded in the relationship matrix during each processing step, without considering the direction of the information flow. Calculating system complexity takes into account the probability that each connection c occurs, considering the number of active entities, resources, and queues in the system. The natural complexity, given by (3), is determined by the active connections and their respective relevance γ, which are calculated based on the sensitivity indices of the parameters in (2), associated with each connection and weighted by the probability that the connection occurs $P(c)$ [28].

$$\psi(c,\gamma) = \sum_{\kappa=1}^{\rho} \left[\gamma_\kappa - P(c_\kappa) \cdot \log_2 P(c_\kappa)\right] \tag{3}$$

System stability refers to its ability to return to equilibrium after disturbances [73]. This involves minimizing internal and external oscillations to achieve a balanced state. To maintain stability, the system requires self-regulation mechanisms to adapt to unexpected changes [29,74]. The ability to maintain equilibrium is important for systems, and Xue et al. [75] and Qiaoge et al. [76] suggest that this can be assessed using specific metrics. Bai and Zhou [77] recommend defining different thresholds for system output when evaluating stability and organizing scenarios within a coincidence detection matrix. Pesterev [31] identifies stable operating ranges, referred to as stability sectors, using concepts from Lyapunov's quadratic functions. Okuyama [30] proposes a method based on mapping trajectories within a state transition matrix to calculate system stability. Finally, the stability metric proposed by Liu et al. [33] enables the calculation of stability indices, detecting parameter configurations that may lead to instability.

The robustness of the system is its ability to maintain functionality in the face of internal and external changes or disturbances [65,73]. When the system deviates from its usual operating pattern, it is considered a disturbance, which introduces uncertainty about its future states [78,79]. According to Klomp et al. [80], robustness can combine both material and symbolic aspects, such as the durability of the equipment and the competence of the operators, respectively. The design of robust systems requires a variety of methods and tools to manage uncertainties and resource constraints, including robust design techniques [81,82]. Lempert and Collins [83] emphasize the importance of identifying diverse scenarios beyond the one optimized for making robust decisions. Schlesinger [84] suggests that in addition to performance, other characteristics of the system can contribute to its robustness. Croskerry [85] stresses that robust design must recognize the vulnerabilities of different scenarios and evaluate the trade-offs between them, which requires the analyst to take careful judgment.

3. Methodology

This section presents the methodology proposed in this work. Initially, the context of the study is established, followed by the introduction of the proposed metrics. The techniques for calculating performance, complexity index, and stability index are detailed, and subsequently, the method for measuring robustness is introduced. Finally, the optimization process to be used in the modeling of the three systems for the case studies is described.

3.1. Contextualization of the proposal

The primary objective of this work is to develop a metric to identify robust solutions among the various possible options. The methodology begins with models of real systems and verifies these models through simulation. In constructing the metric, the concepts of performance, complexity, and stability are utilized to produce the measure of robustness. The approach starts with the system optimized solely for performance. With the optimized input parameters, a baseline value is obtained. Using this baseline, it is possible to construct a spider diagram to perform sensitivity analysis, measure complexity, and formulate the stability metric. Fig. 3 illustrates the flow of the proposed methodology.

The methodology begins with the definition of the baseline scenario c^β, which represents the efficient operation of the system with optimal use of its resources. The determination of c^β can be achieved through an optimization process or by consulting experts. When the optimization process is used to determine c^β, performance metrics are typically used. Fig. 4 illustrates the flow of activities required to calculate performance, using the modeling of the discrete event system.

In Fig. 4, the first step is to obtain and simulate the system model. For discrete event systems, the simulation process and application of the performance metric should be repeated according to the number of replications necessary to eliminate bias. This number can be determined by combining the knowledge of the system with the application of measures of central tendency to the output values obtained from successive replications. The scenario with the best performance after these successive replications is considered the baseline scenario c^β.

The second step is to obtain the sensitivity indices of the parameters considering c^β, which are used in the process of determining the complexity index. The calculation of sensitivity indices is necessary because the chosen complexity metric, which contributes to the robustness metric, is based on connections weighted by these indices. The area method is used to determine the values of the sensitivity indices [28].

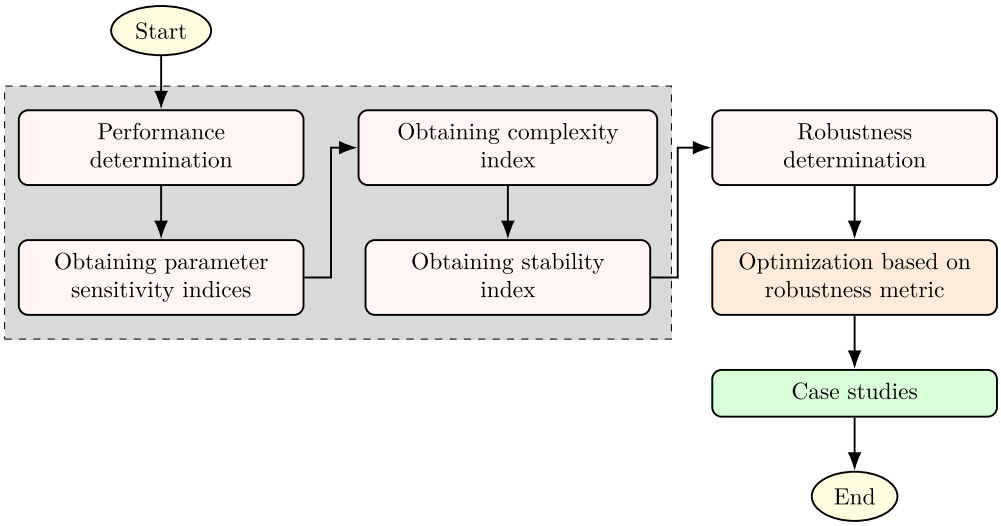

Fig. 3. Flowchart of the proposed methodology.

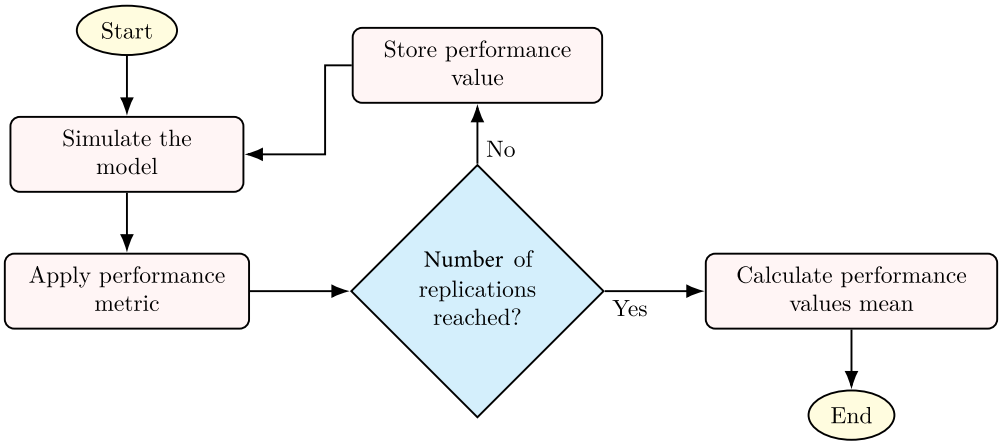

Fig. 4. Flowchart for obtaining the best performance.

3.2. Proposal for natural complexity and stability indices

The third step is the calculation of the natural complexity index i_ψ. This index indicates the degree of proximity between the system's complexity in a given scenario and its natural complexity. The index ranges from $0 \leq i_\psi \leq 1$, decreasing or increasing as the complexity of the scenario diverges from or converges toward the natural complexity. Thus, $i_\psi(c^i)$ is considered the complexity index of scenario c^i, and using (3) as described by Gomes et al. [28], i_ψ is defined by (4). In this context, c^i represents the ith scenario and c^β is the baseline scenario.

$$i_\psi(c^i) = \begin{cases} \dfrac{|\psi(c^i) - 2 \cdot \psi(c^\beta)|}{\psi(c^\beta)} & if \quad \psi(c^i) > \psi(c^\beta) \\ \dfrac{\psi(c^i)}{\psi(c^\beta)} & if \quad \psi(c^i) \leqslant \psi(c^\beta) \end{cases} \tag{4}$$

The proposed stability index is calculated based on the spider diagram, illustrated in Fig. 5, which pertains to the sensitivity analysis of the system with three parameters: x_1, x_2, and x_3. The x-axis represents the percentage variation of each parameter's value relative to its reference value. The y-axis represents the measured system output for each percentage variation of the parameters. It is noted that each line segment of the spider diagram curves exhibits an angle of inclination relative to the horizontal axis, with the first three angles of each curve highlighted.

In general, each of the n curves in the spider diagram can be divided into a different number of points p, resulting in lines $m = p - 1$. This variation occurs because, in the sensitivity analysis process, different ranges of variation may be applied to each input parameter of the system. Thus, for each input parameter x_i of the system, it is possible to determine the vector $\overrightarrow{I_{x_i}} = (\alpha_{i,1}, \alpha_{i,2}, \ldots, \alpha_{i,m})$, which contains the values of the angles formed between the lines of its curve and a line parallel to the x axis.

These vectors can be grouped into the vector $\vec{I} = \left[\overrightarrow{I_{x_1}}, \overrightarrow{I_{x_2}}, \overrightarrow{I_{x_3}}, \ldots, \overrightarrow{I_{x_n}}\right]$, which contains the angles α corresponding to all the curves in the spider diagram. Obtaining $\vec{I}$ is the first step in calculating the stability index. To calculate the angular mean of $\vec{I}$, the arc-tangent function of two parameters is applied to the average of the sines and cosines of the angles contained in $\vec{I}$, as given by:

$$\alpha_{med}(I) = \arctan 2\left(\frac{1}{j}\sum_{i=1}^{j}\sin\alpha_i, \frac{1}{j}\sum_{i=1}^{j}\cos\alpha_i\right) \tag{5}$$

where $\alpha_{med}(I)$ is the angular mean of $\vec{I}$, j is the number of elements in $\vec{I}$, and α_i is the ith angle in $\vec{I}$. Considering the upper limit $\alpha_{max} = 90°$ for the angles contained in $\vec{I}$, the stability index can be calculated by dividing the absolute difference between $\alpha_{med}(I)$ and α_{max} by the value of α_{max}, as given by:

$$\xi = \frac{|\alpha_{med}(I) - \alpha_{max}|}{\alpha_{max}} \tag{6}$$

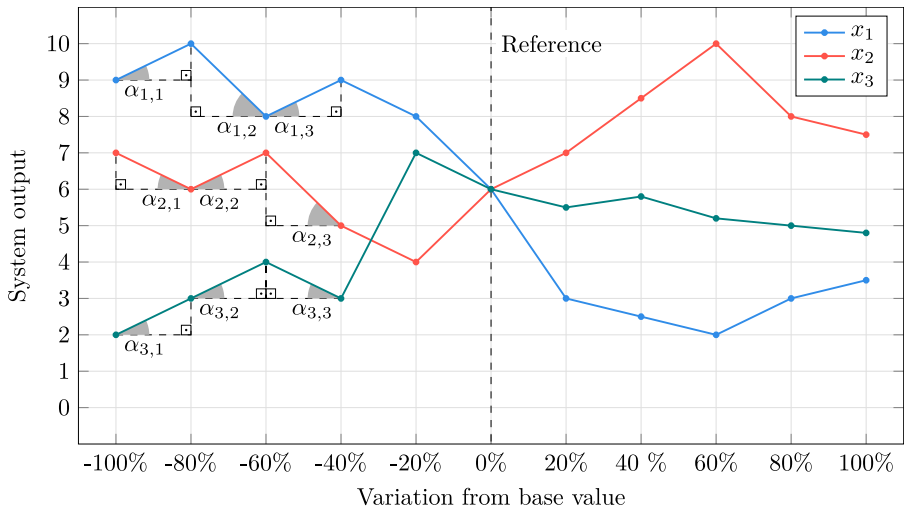

Fig. 5. Spider diagram for a system with three input parameters.

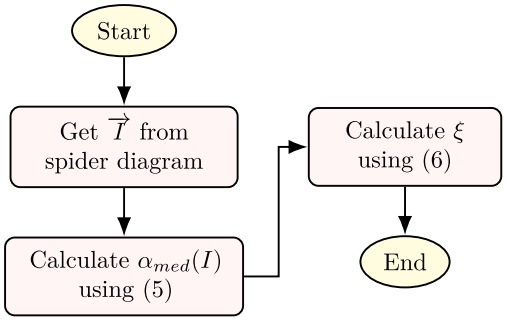

Fig. 6. Flowchart for obtaining the stability index.

The stability value is adjusted to the range $0 \leq \xi \leq 1$, where a higher value of ξ indicates a more stable system in a given scenario. Unlike i_ψ, which has a fixed value for each c^β, the value of ξ can vary within c^β. Fig. 6 illustrates the process for obtaining the proposed ξ.

3.3. Proposal for the robustness metric

The proposed robustness metric integrates all concepts of performance μ_d, complexity i_ψ, and stability ξ. Fig. 7 illustrates the flow for obtaining robustness, highlighting in gray the steps where the values of each of the three components are obtained. The proposed metric is given by:

$$\tau = f(\mu_d + i_\psi + \xi) \tag{7}$$

3.3.1. Mathematical formalization of the proposed model

The proposed robustness metric, τ, is defined as a combination of three fundamental system components: (i) performance μ_d, (ii) complexity i_ψ, and (iii) stability ξ. Its mathematical formulation is expressed in (7), where the function f must satisfy certain mathematical properties to ensure that the metric adequately represents the robustness of the system. Each component must be within the interval $\mu_d, i_\psi, \xi \in [0, 1]$, ensuring comparability and consistency within the integrated metric. Consequently, it follows that:

$$0 \leq \tau \leq 3. \tag{8}$$

The monotonicity property of the metric τ establishes that it must be non-decreasing with respect to each of its components, that is, an increase in any of them must not result in a decrease of the overall metric, as shown in (9). This ensures that improvements in any individual dimension contribute positively to the global robustness value.

$$\frac{\partial \tau}{\partial \mu_d} \geq 0, \quad \frac{\partial \tau}{\partial i_\psi} \geq 0, \quad \frac{\partial \tau}{\partial \xi} \geq 0. \tag{9}$$

The linearity and relative weighting of the metric components can be expressed as a weighted average of the three factors, with adjustable coefficients reflecting the relevance of each criterion, as shown in (10). Here, w_d, w_ψ, and w_ξ are normalized weights such that $w_d + w_\psi + w_\xi = 1$.

$$\tau = w_d \mu_d + w_\psi i_\psi + w_\xi \xi. \tag{10}$$

If no preference is given among the three factors, equal weights are adopted, i.e., $w_d = w_\psi = w_\xi = \frac{1}{3}$, resulting in (11). This formulation ensures the consistency of the metric while allowing for adjustments based on the specific context of the analysis.

$$\tau = \frac{1}{3}(\mu_d + i_\psi + \xi). \tag{11}$$

To verify the consistency of the metric and ensure that τ accurately reflects the robustness of the system, its behavior is analyzed under extreme scenarios: (i) for an ideally robust system, where $\mu_d = i_\psi = \xi = 1$, we have $\tau = \frac{1}{3}(1+1+1) = 1$, (ii) for an extremely fragile system, where $\mu_d = i_\psi = \xi = 0$, we obtain $\tau = \frac{1}{3}(0+0+0) = 0$, and (iii) for a system with imbalanced factors, for example, $\mu_d = 1$, $i_\psi = 0.5$, and $\xi = 0.2$, we have $\tau = \frac{1}{3}(1+0.5+0.2) = 0.5667$. This illustrates that the metric adequately captures the heterogeneity of the characteristics of the system.

Traditional metrics often evaluate performance, complexity, and stability separately. For example, the efficiency metric μ_d ignores structural complexity and system resilience, the structural complexity metric i_ψ does not account for operational stability, and the stability metric ξ does not consider the impact of performance and complexity. By integrating these three elements, the metric τ enables a more balanced assessment that is better aligned with the characteristics of complex systems.

3.4. Optimization using the robustness metric

The optimization process determines the values of the parameters of a given scenario c^a and presents them to the simulator, which then calculates the performance $\mu_d(c^a)$, the natural complexity indices $i_\psi(c^a)$, and the stability $\xi(c^a)$. In this process, the value of $\tau(c^a)$ in (7) is considered the evaluation function f_{eval} of the optimization process.

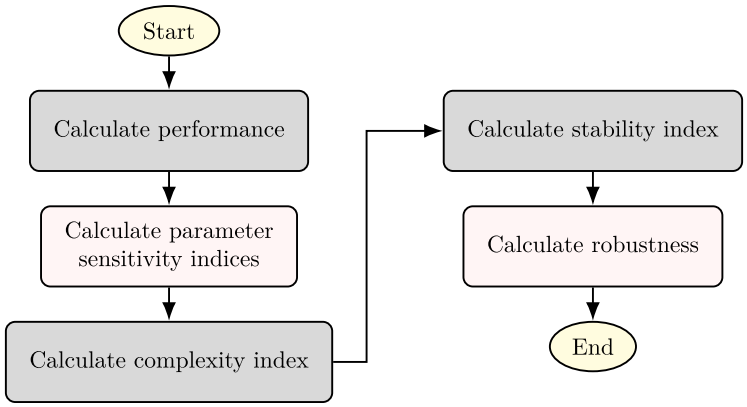

Fig. 7. Flowchart for obtaining the proposed robustness metric.

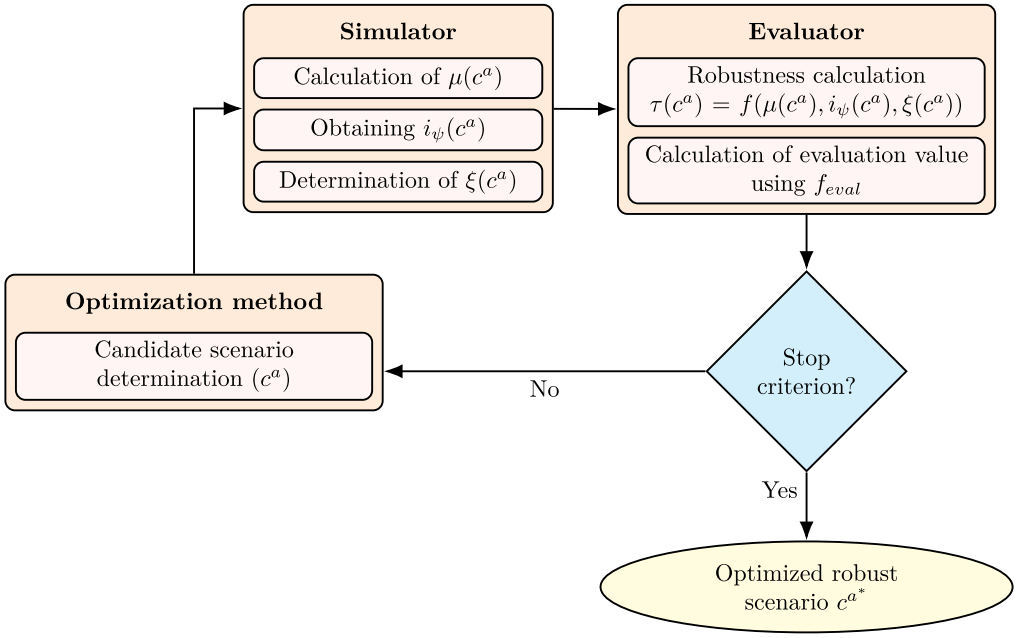

Fig. 8. Flowchart of the optimization process based on the robustness metric.

Taking into account values in the range $0 \leq \tau \leq 1$ for each component of the robustness metric, the maximum possible value is $f_{eval} = 3$. Since higher values of $\mu_d(c^a)$, $i_\psi(c^a)$, and $\xi(c^a)$ are preferable, the problem can be defined as a maximization problem. Using algebraic manipulation, the maximization problem can be transformed into a minimization problem, and thus the evaluation function is defined as:

$$f_{aval} = \frac{1}{\tau(c^a)} \tag{12}$$

Fig. 8 illustrates the flow of the optimization process, where the optimized scenario c^{a^*} is obtained at the end of the process. Even if the system does not achieve the highest values for μ_d, i_ψ, and ξ, the system is guided to operate robustly when the optimized values for the input parameters are used, encompassing performance, complexity, and stability aspects together.

4. Models for case studies

To apply the proposed methodology, three well-established and distinct systems from the literature are used. All systems are modeled using discrete event systems. The first model is an intensive care unit system, the second model is a process scheduling system, and the third model is an electric vehicle traction and braking system.

4.1. Intensive care unit system

An intensive care unit (ICU) is a dedicated space for patients who require constant supervision and medical care. In addition to healthcare professionals, this environment is equipped with devices that support the functioning of vital systems in the body during the treatment of serious diseases [86]. Various procedures are performed in the ICU, including adverse events that may result in extended hospitalization, disability, or death, caused by incompetence, negligence, or accidents in healthcare delivery. The occurrence of adverse events burdens the ICU system as a whole, increasing both financial costs and psychological impacts.

The ICU system model is described in detail by Gomes et al. [28] and illustrated in Fig. 9. When an ICU bed is requested, the patient waits in a priority-based first-in, first-out (FIFO) queue until the necessary resources are available and the intensivist confirms admission. If accepted, the resources are allocated to the patient, who is then admitted to the system. If denied, the bed request is canceled. When the patient is discharged, either due to recovery or death, the resources are relocated.

The parameters considered in this ICU model are: (i) number of beds, (ii) percentage of supplies, (iii) percentage of medical personnel, (iv) arrival rate, and (v) adverse event rate. The performance of the

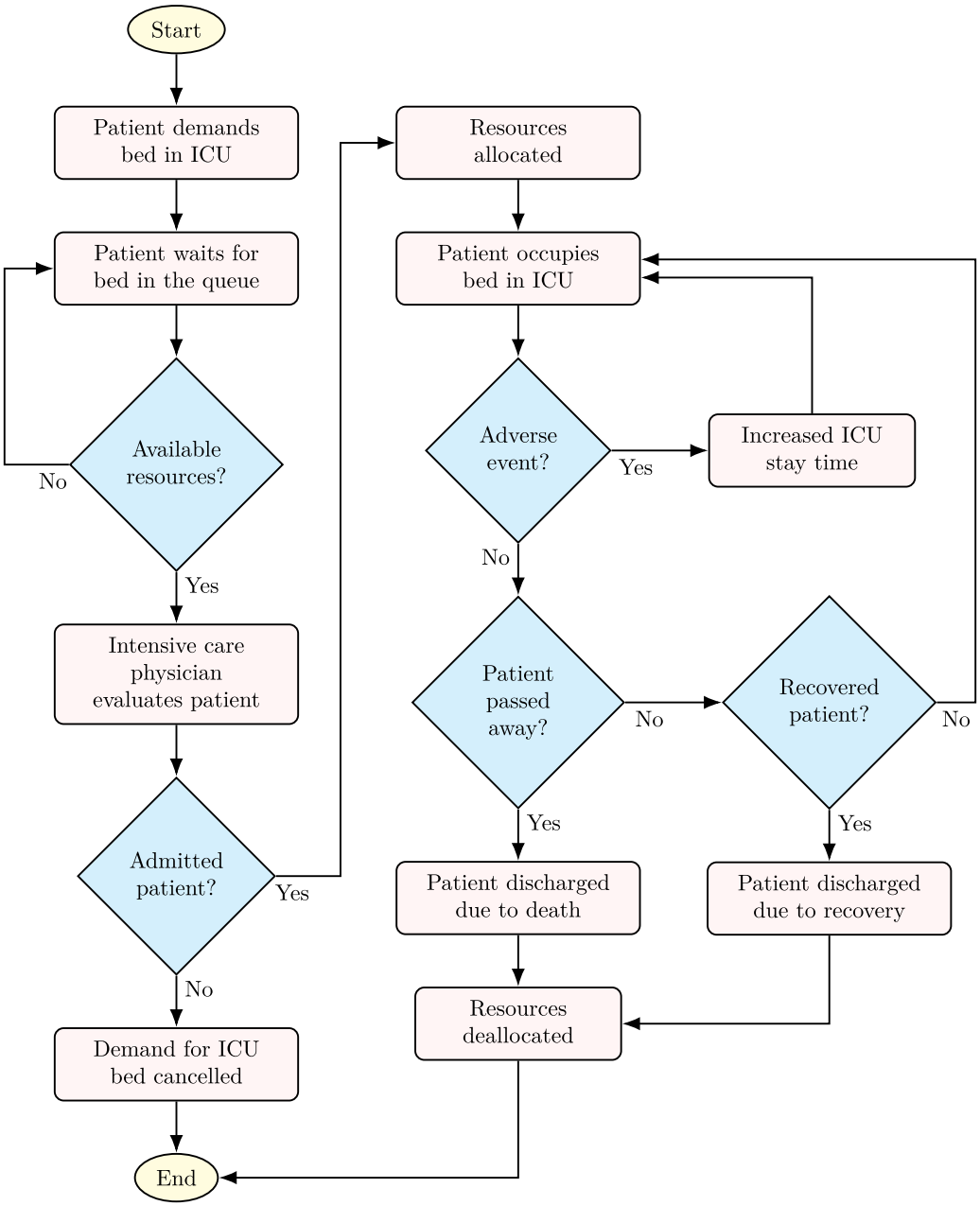

Fig. 9. Flowchart of the ICU model.

ICU model is calculated based on the relationship between the number of admissions n_a, the average length of stay t_s, the average number of patients in the queue n_{pf}, and the average number of beds in use n_l, as given by (13), where $\mu_d(U)$ represents the performance of the ICU system, and $n_{a_{ref}}$, $t_{s_{ref}}$, $n_{pf_{ref}}$, and $n_{l_{ref}}$ correspond to the reference values for n_a, t_s, n_{pf} and n_l, respectively. The complexity of the ICU system is determined based on the relationships between patients and the elements of the system. Fig. 9 illustrates these relationships.

$$\mu_d(U) = \frac{1}{4} \cdot \left(2 + \frac{n_a}{n_{a_{ref}}} - \frac{n_{pf}}{n_{pf_{ref}}} + \frac{n_l}{n_{l_{ref}}} - \frac{t_s}{t_{s_{ref}}} \right) \tag{13}$$

4.2. Process scheduling system

The process scheduling (PS) system is the part of the operating system that coordinates the execution of processes during computer usage [87]. In modeling the system, processes are considered entities that utilize the following resources: (i) central processing unit (CPU), (ii) random access memory (RAM), (iii) input/output devices, and (iv) hard drives (HD). The concept of quantum is used, which determines the maximum CPU usage time allowed per process [88]. When a process's CPU usage time reaches the quantum value, its execution is interrupted. The interrupted process must wait for another opportunity to use the CPU.

The flow illustrated in Fig. 10 represents the system's dynamics. The first steps are: (i) creating the process, (ii) waiting for RAM availability in a FIFO queue, (iii) waiting for CPU availability in a priority-ordered FIFO queue, and (iv) executing the process at the front of the queue until either the quantum value is reached, the process requires an input/output device or HD, or its CPU demand is met. The flow proceeds as follows: (i) if the process execution is interrupted due to the need for an input/output device or HD, the process is sent to the corresponding resource queue, (ii) when the input/output device or HD becomes available, the first process in the respective queue uses the

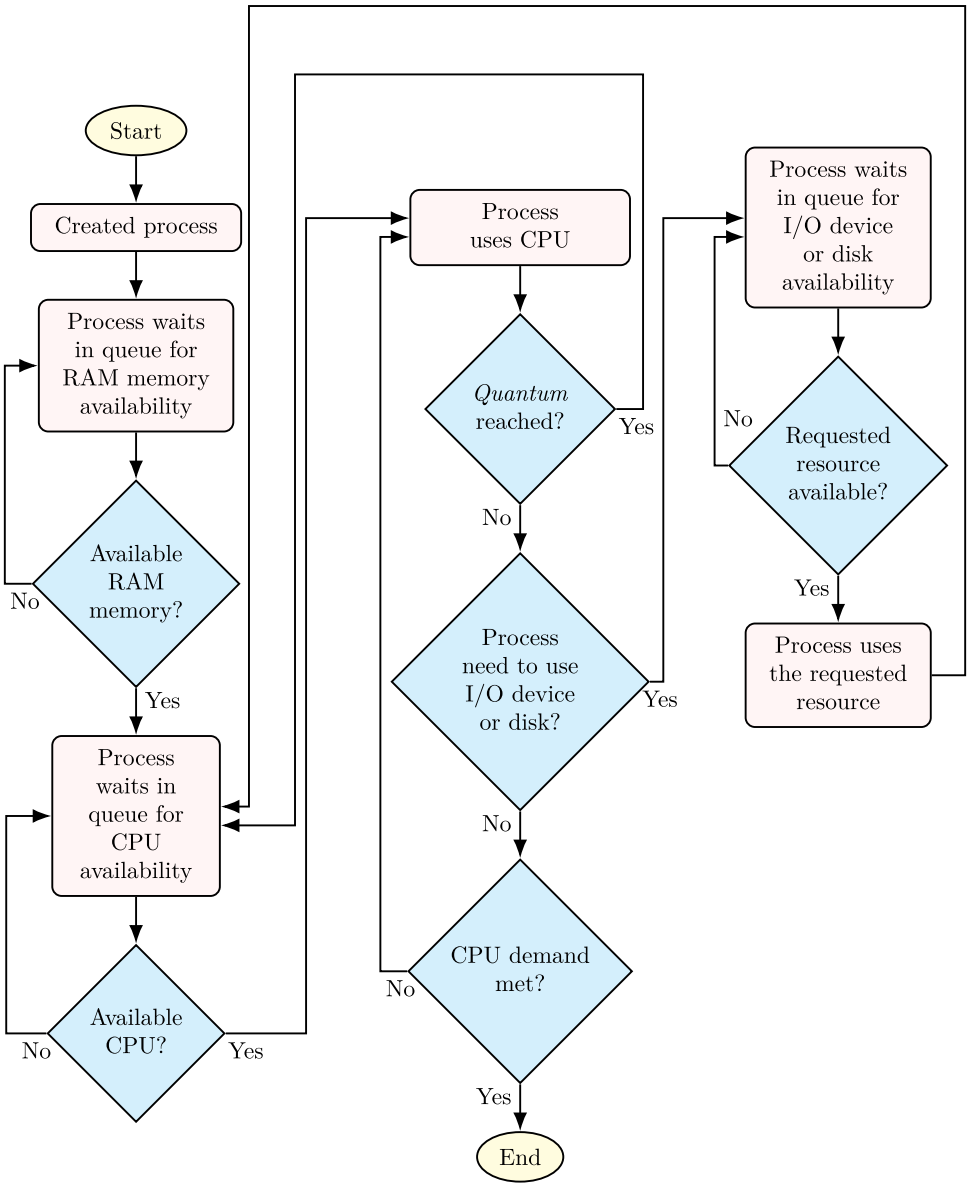

Fig. 10. Flowchart of the PS model.

resource, and (iii) processes that either finish execution due to reaching the quantum or complete the use of input/output devices or HD are returned to the CPU waiting queue.

The states defined for the processes are: (i) created, (ii) in queue for RAM usage, (iii) in queue for CPU usage, (iv) in queue for input/output device or HD usage, (v) using CPU, (vi) using input/output device or HD, and (vii) finished. The modeled events are: (i) process creation, (ii) RAM allocation, (iii) CPU usage, (iv) input/output device or HD usage, (v) processing interruption due to quantum exhaustion, (vi) processing interruption for input/output device or HD access, (vii) process completion, (viii) RAM deallocation, (ix) CPU deallocation, and (x) input/output device or HD deallocation.

The modeled parameters are: (i) number of CPUs, (ii) amount of RAM, (iii) number of input devices, (iv) number of output devices, and (v) number of HDs. Unlike traditional metrics, the proposed metric for calculating the performance of the PS system is based on: (i) the ratio between the amount of work demanded and the amount of work completed, as proposed by Lynch [89] and Sacha [90], (ii) the percentage of resource utilization: CPU by Kung et al. [91] and Menezes et al. [92], RAM by Chen & Bershad [93] and Kayande & Shrawankar [94], input and output devices by Page [95] and Priem & Rosenthal [96], and HD by Katz et al. [97] and Guo et al. [98], and (iii) the waiting time of processes in system queues by Cutler & Lenzmeier [99], Bohm et al. [100], Pierre [101], and Shah et al. [102]. Thus, the performance of the PS system is given by:

$$\mu_d(E) = \frac{1}{(2 \cdot z) + 1} \cdot \left[\frac{p_f}{p_g} + \sum_{i=1}^{z} u_{r(i)} + \left(1 - \frac{tf_{r(i)}}{\max\left(tf_{r(i)}\right)} \right) \right] \tag{14}$$

where $\mu_d(E)$ is the performance, p_f is the number of completed processes, p_g is the number of processes generated during the simulation, z is the number of system resources, $u_{r(i)}$ is the percentage of utilization of the ith system resource, $tf_{r(i)}$ is the average waiting time in the queue for the ith system resource, and $\max(tf_{r(i)})$ is the longest average waiting time in the queue for the ith system resource.

Fig. 11 illustrates the flow of the PS model, in which there are nine processes in the system: P_1 to P_9. When a process uses the CPU, input devices, output devices, or HD, processes P_1 to P_4, with connections C_1 to C_8, two connections are taken out per process: one with the resource and one with RAM. If the process is waiting in a queue for the release of a resource, except for RAM, two connections are also counted per

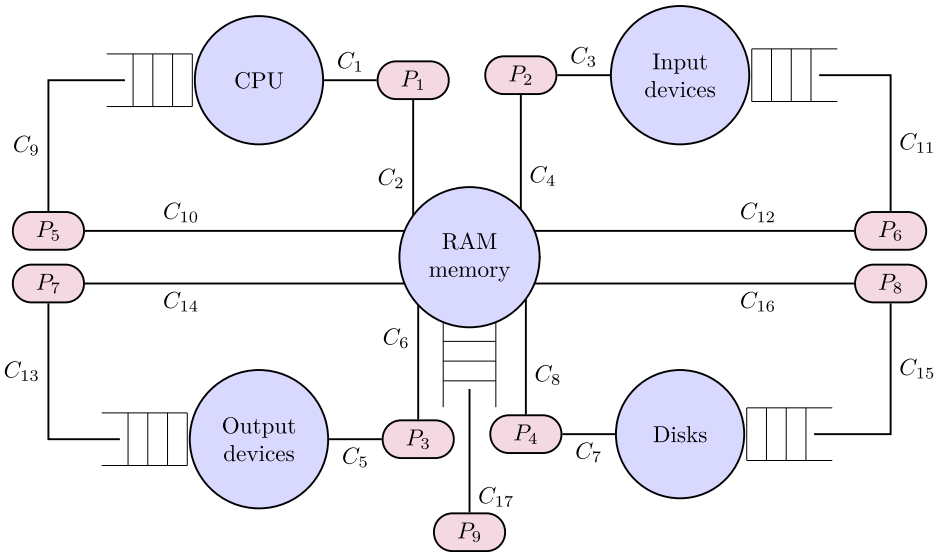

Fig. 11. Diagram of the scheduling system with nine processes.

process: one with the queue of the required device and one with RAM, processes P_5 to P_8, with connections C_9 to C_{16}. Furthermore, if the process is waiting in a queue for RAM to be released, process P_9, with connection C_{17}, only one connection is accounted for.

4.3. Electric vehicle traction and braking system

The electric vehicle (EV) traction and braking system is a key area of research to improve energy conservation and battery efficiency [103, 104]. Fig. 12 illustrates the components and connections considered in the modeling of this system with an electric machine. Near each connection, the following representations are shown: (i) control connection between components `C`, (ii) electrical connections in direct current (DC) and alternating current (AC), labeled as `CC` and `CA`, respectively, and (iii) torque connection `T`.

Fig. 12 illustrates the diagram of the electric vehicle (EV) system, where the blue arrows indicate traction. In this scenario, the accelerator pedal communicates with the system controller, which sends the desired speed to the DC/AC inverter. The alternating current is supplied to the electric machine which operates as a motor. Finally, the power from the electric machine, converted into torque, is transferred to the EV's wheels. The red arrows indicate braking. In this case, the brake pedal communicates with the system controller, which informs the regenerative braking system of the desired deceleration rate. During braking, the kinetic energy from the inertial motion of the wheels forces the electric machine to rotate in the opposite direction, causing it to function as a generator and recharge the batteries. The green arrows indicate the external energy source used to charge the batteries.

Taking into account the direction of the arrows in Fig. 12, seven connections occur in the system during traction. During braking, eleven connections are involved. If the electric vehicle (EV) has more than one electric machine and the urban or sport driving modes are activated during the simulation, the connections between the additional machines and their adjacent elements must be taken into account [105]. Thus, if the EV is in traction mode, an additional two connections should be considered for urban mode or six additional connections for sport mode. If the EV is in regenerative braking mode and the urban or sport driving modes are activated, four or twelve additional connections should be counted, respectively. When the system is in battery charging mode from an external source, seven connections are considered.

When using two or four electric machines, each is installed on one axle of the vehicle or on the wheels, respectively. The modeled electric vehicle (EV) features the following driving modes: (i) economical, where only one electric machine is activated on the front axle, (ii) urban, where two machines are activated on both axles, and (iii) sport, where four machines are activated on the wheels [106]. The flow of actions modeled for the electric vehicle traction and braking (EVTB) system is illustrated in Fig. 13. The model considers the following states: (i) traction, (ii) braking, (iii) battery charging from an external source, and (iv) off. The modeled events are: i) activation of the EV, (ii) charging of the battery pack from an external source, (iii) selection of driving mode, (iv) traction operation, (v) regenerative braking operation, (vi) interruption of battery charging from an external source, (vii) shutdown of the EV due to battery depletion, and (viii) shutdown of the EV at the driver's request. The movement of the EV is influenced by the following forces: (i) rolling resistance, (ii) aerodynamic resistance, iii) incline resistance, and (iv) inertial forces.

The modeled parameters are: (i) battery power, (ii) electric machine power, and (iii) number of electric machines. After simulating the model, the performance of the system is calculated based on battery consumption and the range of the electric vehicle (EV), as given by (15). In this expression, $\mu_d(V)$ represents the performance of the EVTB system, c_{med} is the average battery consumption during the trip, c_{max} is the maximum battery consumption recorded during the trip, a_r is the range of EV, calculated based on the remaining battery level and average consumption, and a_{ref} is the reference range defined by the manufacturer of the EV.

$$\mu_d(V) = \frac{1}{2} \cdot \left(\frac{c_{med}}{c_{max}} + \frac{a_r}{a_{ref}} \right) \tag{15}$$

5. Results

In this section, the results obtained from applying the proposed methodology to the case study models are presented. Computational experiments were conducted to calculate all the variables necessary to determine the robustness of the systems. Following the presentation of the results, a comprehensive discussion of the findings is provided. Fig. 14 illustrates the process used to present the results for each case study. Initially, the baseline scenario c^{β} for each model is presented. Then, the configurations for each model are determined, which refer to the specifications kept constant throughout all simulations. After defining the configurations, the optimization process based on the proposed robustness metric is carried out and the optimized scenarios are presented. Finally, an analysis of the scenarios for each model is performed.

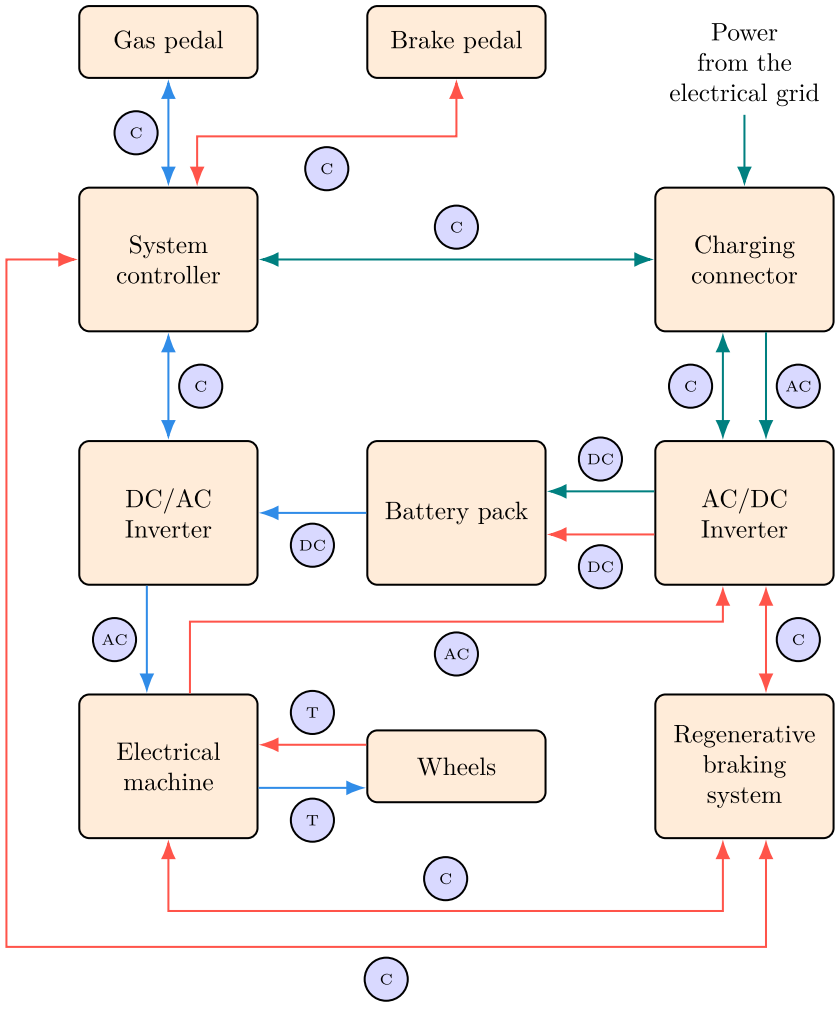

Fig. 12. Diagram of the electric vehicle traction and braking system.

To ensure the reliability and feasibility of computational experiments, simulation intervals were defined based on two main criteria: (i) the operational relevance of the systems, with ranges established to encompass both typical and extreme scenarios, allowing the evaluation of system behavior under varying conditions, and (ii) the feasibility of conducting the experiments, with adjustments made to ensure that processing time remained compatible with available computational resources without compromising result accuracy. Preliminary tests were performed to determine the minimum number of replications required to obtain statistically significant results.

For the ICU model, the simulation period was set to 365 days, reflecting a full annual operating cycle, including seasonal effects and variations in patient arrivals. For the PS model, a 24-h simulation period was adopted to capture fluctuations in processing demand over the course of a typical operational day. Finally, in the EVTB model, the simulation interval corresponded to complete driving cycles, including acceleration and braking under real-use conditions, with variations in terrain.

5.1. Determination of c^{β} and parameterization of the ICU model

The base case c^{β} for the ICU problem was defined based on the study by Gomes et al. [28], which indicates that the configuration $c^{\beta} = (10,\ 100,\ 105,\ 12,\ 36)$ represents a typical scenario for this type of system, validated by healthcare specialists. This scenario was considered the most efficient in terms of hospital resource utilization and patient demand. It corresponds to a regular operating condition in which the ICU operates with 10 beds, 100% of resources, 105% of medical staff (including an additional 5% due to partial shift overlap in specific cases), an adverse event rate of 12%, and a patient arrival rate of $T_C = 36$ h. The performance value calculated for c^{β} was $\mu_d = 0.7288$, obtained as the average of the results of 100 simulation replications, as defined by (13). This base case was used as the foundation for the subsequent simulations.

The simulations conducted with the ICU model followed the same configurations as those adopted by Gomes et al. [28]. For each patient who arrived at the ICU during 365 days of simulation, a priority was assigned as follows: 35% of patients had **Priority 1**, 50% had **Priority 2**, 7% had **Priority 3**, 7% had **Priority 4**, and 1% had **Priority 5**. Patients waited for treatment in a FIFO queue organized by their priority, from **Priority 1** to **Priority 5**. When resources were available, the intensivist evaluated the first patient in the queue, with a 10% refusal rate for admission, in which case the patient did not enter the ICU room. When a patient was accepted, the following allocations were made: (i) a bed, (ii) between 6% and 12% of the total resources, following a uniform distribution $U(6;\ 12)$, and (iii) between 6% and 12% of the working hours of the medical personnel, also following a uniform distribution $U(6;\ 12)$.

The average length of stay for patients in the ICU, in days, is defined according to their priority. Assuming a normal distribution, the following parameters were adopted: **Priority 1** with $N(8;3)$, **Priority 2** with $N(5;2)$, **Priority 3** with $N(7;1)$, **Priority 4** with $N(7;1)$, and **Priority 5** with $N(30;\ 7)$. During their stay in the ICU, each patient involved in an adverse event has their stay extended by an additional 15 to 45

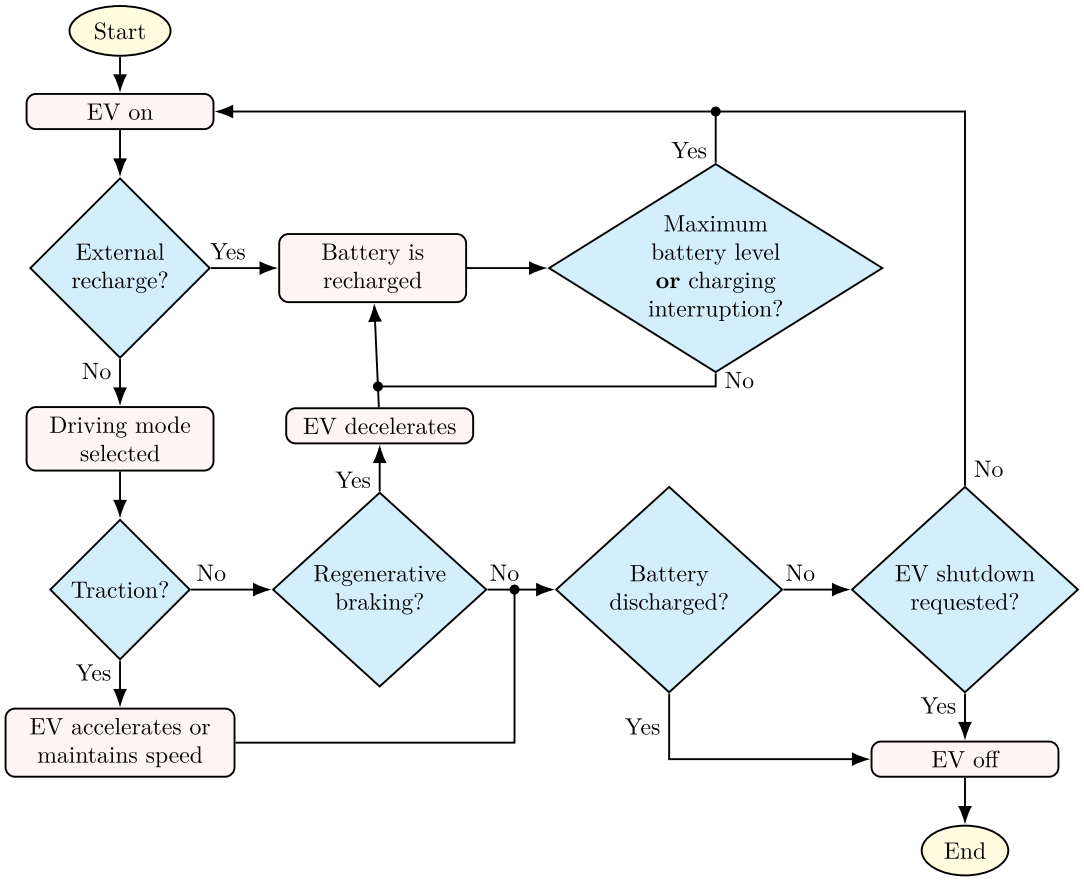

Fig. 13. Diagram of the electric vehicle traction and braking system.

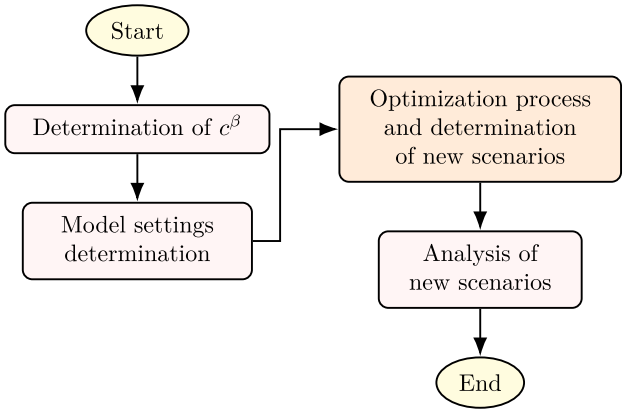

Fig. 14. Flow of results for each studied model.

days, following a uniform distribution $U(15;\ 45)$, with a probability of death 20%. Whether due to death or recovery, when a patient is discharged from the ICU, the allocated resources are freed up. Patients discharged are classified as follows: (i) recovered without a history of adverse events, (ii) deceased without a history of adverse events E_A, (iii) recovered with a history of adverse events, and (iv) deceased with a history of adverse events.

5.1.1. Application of the robustness metric in the ICU model

The application of the proposed robustness metric to the ICU model allowed studies related to unit resource size: beds n_L, supplies p_I, and medical staff p_{EQ}, which are used to meet the demand for care, established by patient arrival rates T_C and adverse event rates t_{EA}. The metric application also allowed for an examination of robustness behavior when parameter values were varied. The variation in robustness is related to: (i) the number of admissions to the unit, length of stay, size of the admission queue and number of beds in use, (ii) the dynamics of the unit, considering its connections, and (iii) the ability to maintain equilibrium when the quantity of hospital resources and the rates determining care demand are altered. To obtain scenarios with robustness greater than c^{β}, an optimization process was performed using the particle swarm optimization (PSO) algorithm with a swarm of 20 particles, as described in (12). The lower and upper bounds used for parameter values in the optimization were given by:

$$M_{lim} = \begin{bmatrix} n_{L_l} & n_{L_u} \\ p_{I_l} & p_{I_u} \\ p_{EQ_l} & p_{EQ_u} \\ t_{EA_l} & t_{EA_u} \\ t_{C_l} & t_{C_l} \end{bmatrix} \tag{16}$$

where n_{L_l} and n_{L_u} are the lower and upper bounds of n_L, p_{I_l} and p_{I_u} are the lower and upper bounds of p_I, p_{EQ_l} and p_{EQ_u} are the lower and upper bounds of p_{EQ}, t_{EA_l} and t_{EA_u} are the lower and upper bounds of t_{EA}, and t_{C_l} and t_{C_u} are the lower and upper bounds of t_C, as presented in Table 1, where the subscript $_l$ denotes the lower bound and the subscript $_u$ denotes the upper bound.

The stopping criteria adopted in the optimization process were: the maximum number of iterations of the method, $i_{t_{max}} = 100$, or an evaluation function value below $f_{aval} < 10^{-6}$. The inertia coefficient w was calculated in each iteration based on (17), with $w_{max} = 1.2$ and $w_{min} = 0.9$, to balance global and local exploration during optimization. For particle acceleration coefficients, values of $c_1 = 1.5$ for the cognitive term and $c_2 = 0.5$ for the social term were used. The choice of a higher value for the cognitive term, relative to the social term, is justified by

Table 1
Lower and upper limits used for parameter values in the optimization of the ICU model.

Parameters	Limits	
n_L	n_{L_l} 1	n_{L_u} 20
p_I	p_{I_l} 15	p_{I_u} 200
p_{EQ}	p_{EQ_l} 15	p_{EQ_u} 200
t_{EA}	t_{EA_l} 5	t_{EA_u} 24
t_C	t_{C_l} 15	t_{C_u} 50

Table 2
Relevance factors and probabilities of occurrence for each type of connection in the ICU model.

Type of connection	γ	$P(c)$
Patient – priority Queue	S^a_C	Experimental probability
Patient – bed	S^a_L	$1/n_L$
Patient – supplies	S^a_I	0.9
Patient – medical team	S^a_{EQ}	0.9
Patient – adverse event	S^a_{EA}	$1/t_{EA}$

the nature of the ICU model optimization problem, which presents a multimodal search space with multiple near-optimal solutions. The ICU system parameters were adjusted within ranges that reflect the actual operational capacity of this type of unit. The number of beds ranged from 1 to 20, the availability of supplies and medical personnel ranged from 15% to 200%, the adverse event rate was established between 5% and 24%, and the patient arrival rate ranged from 15 to 50 h.

$$w = w_{max} - \frac{w_{max} - w_{min}}{i_{t_{max}}} \cdot i_t \tag{17}$$

in which i_t is the current iteration number. Based on various experiments, such as those by Sun & Xiong [107], values in the range of [0.9, 1.2] are proposed for w_{min} and w_{max}, respectively. The calculation of each component of the metric was performed during the optimization, allowing the robustness value of each evaluated scenario to be determined. Performance was calculated using (13), with 100 replications carried out for each scenario. To assess the complexity of the scenarios evaluated during optimization, it was necessary to obtain sensitivity indices for each scenario, the probabilities of occurrence for each type of connection and their respective relevance factors.

The sensitivity indices for each scenario were calculated considering: (i) the parameter values of the scenario as reference values, (ii) a variation range of $[-90\%, 100\%]$ for the parameter values, constrained by the lower and upper limits presented in Table 1, and (iii) an analysis interval of $[-90\%, 100\%]$. For each scenario evaluated, the connection probabilities $P(c)$ provided in Table 2 were used. Table 2 shows the relevance factors γ for each type of connection in the model, where S^a_C, S^a_L, S^a_I, S^a_{EQ}, and S^a_{EA} are the sensitivity indices for the model parameters. The complexity of the scenarios, weighted by the relevance factors, was calculated using the probabilities listed in Table 2. The complexity index for each scenario was calculated using (4). The stability indices for each scenario evaluated during optimization were calculated using (6).

After completing the optimization process, five scenarios with a τ value higher than that calculated for c^β were identified. The best swarms, the quantities of resources for each scenario, the percentage of adverse events E_A, the arrival rate T_C, the optimization robustness index, the performance and the complexity are detailed in Table 3. Each particle c^{a_i} in the swarm, where $i = 1, 2, \ldots, 20$, represents a distinct scenario. The sensitivity, stability, complexity, and robustness indices for each of the five scenarios are provided in Table 4.

Table 3
Best swarms, resources, arrival rate, robustness index, performance and complexity of the ICU model.

c^{a_i}	Bed	Supplies	Team	E_A [%]	T_C [h]	$\tau(c^{a_i})$	$\mu_d(c^{a_i})$	$\psi(c^{a_i})$
$c^{a_{19}}$	13	122	97	11	35	0.8921	0.7279	25.32
c^{a_8}	11	127	141	11	30	0.8912	0.7211	25.06
c^{a_5}	11	138	137	10	39	0.8897	0.7110	25.89
c^{a_4}	9	130	122	9	37	0.8803	0.7002	24.33
$c^{a_{20}}$	12	109	112	10	28	0.8797	0.6998	24.93

Table 4
Sensitivity, stability and complexity indices for the ICU model.

c^{a_i}	S^a_L [%]	S^a_I [%]	S^a_{EQ} [%]	S^a_{EA} [%]	S^a_C [%]	$\xi(c^{a_i})$	$i_\psi(c^{a_i})$
$c^{a_{19}}$	40.09	9.16	3.76	20.23	26.76	0.9532	0.9861
c^{a_8}	5.81	27.06	30.27	4.85	32.01	0.9609	0.9914
c^{a_5}	13.36	24.09	31.13	1.68	29.74	0.9822	0.9757
c^{a_4}	30.11	2.08	20.31	30.75	16.75	0.9782	0.9624
$c^{a_{20}}$	16.47	3.27	31.68	11.84	36.74	0.9532	0.9861

5.1.2. Analysis of scenarios for the ICU model

The multidimensional nature of the robustness metric allows both quantitative studies that focus solely on robustness and qualitative studies that consider the value of each component of the metric. Fig. 15 shows the amount of resources for the eight scenarios with the highest robustness values identified after the optimization process for the ICU model on the x-axis. The y-axis represents the performance values μ_d, the complexity index i_ψ, the stability index ξ and the robustness τ for each scenario.

In the qualitative analysis, it is observed that the performance value of c^β was the highest obtained, with the ICU satisfactorily meeting the demand of patients and effectively using the available hospital resources. The μ_d values measured in scenarios with a higher τ than that recorded for c^β were slightly lower than the μ_d value measured for c^β, with a minimal increase as τ increases. The three scenarios with τ values greater than that of c^β and higher μ_d values were $(13, 122, 97, 11, 35)$, $(11, 127, 141, 11, 30)$ and $(11,\ 138,\ 137,\ 10,\ 39)$. In scenarios with high μ_d values: (i) the number of admitted patients was high, (ii) the average length of stay in the ICU was reduced, (iii) the number of patients waiting for a bed in the ICU was reduced, and (iv) the occupancy rate of the bed was close to 85%.

In the qualitative analysis, it is observed that the highest value i_ψ was found for c^β, as this scenario serves as the reference for the index. The three scenarios with τ values greater than that recorded for c^β, which had the highest i_ψ values, were $(13, 122, 97, 11, 35)$, $(11, 127, 141, 11, 30)$, and $(12, 109, 112, 10, 28)$. In contrast to the values μ_d and i_ψ, the value ξ for c^β was the lowest recorded. The scenarios with values of τ higher than those of c^β and with the highest values of ξ were $(11, 138, 137, 10, 39)$, $(9, 130, 122, 9, 37)$, and $(11, 127, 141, 11, 30)$.

Considering both the quantitative and qualitative analyzes, the following scenarios stand out: (i) $(12, 109, 112, 10, 28)$, which has the third highest i_ψ and is the fifth highest in τ, (ii) $(9, 130, 122, 9, 37)$, which has the second highest ξ and is the fourth highest in τ, (iii) $(11, 138, 137, 10, 39)$, which has the third highest μ_d and the highest ξ, being the third highest in τ, (iv) $(11, 127, 141, 11, 30)$, which has the second highest μ_d and i_ψ values and the third highest ξ, making it the second highest in τ, and (v) $(13, 122, 97, 11, 35)$, which has the highest μ_d and i_ψ values, being the scenario with the highest τ. Examining the two scenarios with the highest τ values, it shows that the scenario $(11, 127, 141, 11, 30)$ has the highest ξ, while the scenario $(13, 122, 97, 11, 35)$ has the highest values μ_d and i_ψ. The relevance level assigned to each component of the metric should guide the final choice between the scenarios by the analyst.

5.2. Determination of c^β and parameterization of the PS model

For the PS model, the base case parameter values c^β were determined through Monte Carlo optimization, considering 20,000 possible

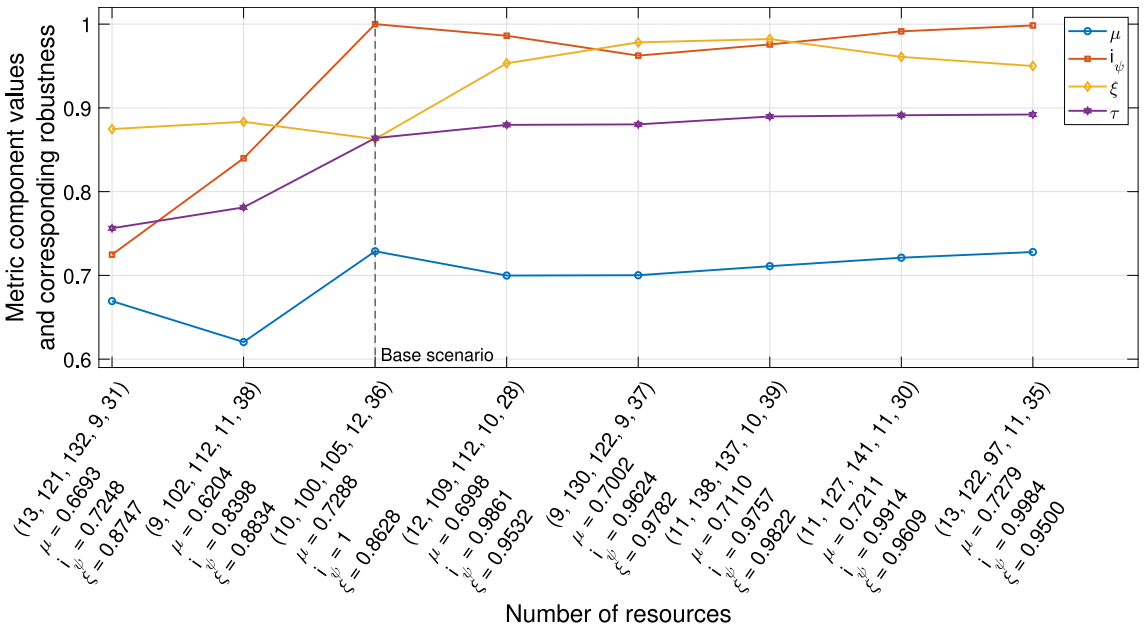

Fig. 15. Components of the metric and robustness × resource quantities for the ICU model.

combinations. The configuration $c^{\beta} = (4,\ 32,\ 2,\ 2,\ 2)$ was identified as the most efficient based on the performance metric. Consequently, four processing units, 32 megabytes [MB] of RAM, two input devices, two output devices, and two hard drives are assumed to constitute the computational resource configuration that adequately meets the demand for the problem. The performance value obtained for c^{β} was $\mu_d = 0.8271$, corresponding to the average of the results from 100 simulation replications, as defined in (14).

The random sample yielded a standard deviation of 0.2388 and a total error rate of $\epsilon = 0.005$. The variables considered were: number of processing units n_{CPU}, amount of RAM t_{RAM}, number of input devices n_{DE}, number of output devices n_{DS}, and number of hard drives n_D. The lower and upper bounds used for the parameter values during the optimization process were:

$$M_{lim} = \begin{bmatrix} n_{CPU_l} & n_{CPU_u} \\ t_{RAM_l} & t_{RAM_u} \\ n_{DE_l} & n_{DE_u} \\ n_{DS_l} & n_{DS_u} \\ n_{D_l} & n_{D_u} \end{bmatrix} \tag{18}$$

where n_{CPU_l} and n_{CPU_u} are the lower and upper limits of n_{CPU}, t_{RAM_l} and t_{RAM_u} are the lower and upper limits of t_{RAM}, n_{DE_l} and n_{DE_u} are the lower and upper limits of n_{DE}, n_{DS_l} and n_{DS_u} are the lower and upper limits of n_{DS}, and n_{D_l} and n_{D_u} are the lower and upper limits of n_D, as listed in Table 5, where the subscript $_l$ denotes the lower limit and $_u$ denotes the upper limit.

The same configurations for the PS model were maintained in all simulations. A simulation period of 24 h was considered, with new processes created every 300 ms on average, following a normal distribution $N(300;\ 60)$. Regarding processing demand, each created process required CPU usage for an average of 1.2 s, with a normal distribution $N(1.2;\ 0.36)$. The amount of RAM needed to allocate each process, $t_{RAM_{proc}}$, was on average 2 MB, with a normal distribution $N(2;\ 1)$. Each generated process was assigned a priority that determines its position in the FIFO queue of processes that wait for CPU availability. The priority distribution was as follows: 1% with **Priority 1**, 7% with **Priority 2**, 7% with **Priority 3**, 35% with **Priority 4**, and 50% with **Priority 5**, where lower priority precedes higher priority.

The maximum allowed CPU usage time (*quantum*) per process was set to 200 ms, and the probability of a process requiring input/output devices or HD usage during its execution was fixed at 5%. Normal distributions were used for the usage time (in seconds) of the input devices, output devices, and HD by processes, with parameters $N(3;\ 0.3)$, $N(5;\ 0.5)$, and $N(2;\ 0.3)$, respectively.

Table 5
Lower and upper limits used for evaluating the performance of the PS model.

Parameters	Limits	
n_{CPU}	n_{CPU_l} 1	n_{CPU_u} 8
t_{RAM}	t_{RAM_l} 4	t_{RAM_u} 64
n_{DE}	n_{DE_l} 1	n_{DE_u} 4
n_{DS}	n_{DS_l} 1	n_{DS_u} 4
n_D	n_{D_l} 1	n_{D_u} 4

5.2.1. Application of the robustness metric in the PS model

The application of the proposed robustness metric to the PS model allowed an analysis of the computational resources required to meet a given processing demand. This application allowed for examination of robustness behavior as parameter values varied. The robustness variation is related to: (i) the ratio of completed processes to demanded processes, considering resource utilization and process queue time, (ii) the connections made during the PS dynamics, and (iii) the ability to maintain balance when processing power is altered. To obtain scenarios with greater robustness than c^{β}, an optimization process was performed using the PSO algorithm, with the evaluation function given by (12). The swarm consisted of 15 particles, and the lower and upper limits used for the parameter values in optimization are specified in Table 6.

The stopping criteria for the optimization process were: the maximum number of iterations, $n_{iter} = 50$, or a value of the evaluation function below $f_{aval} < 10^{-6}$. The inertia coefficient w was calculated at each iteration of the method, as defined in (17), with $w_{max} = 1.2$ and $w_{min} = 0.9$. Equal values were adopted for the particle acceleration coefficients $c_1 = c_2 = 2.0$, in order to assign equal importance to local and global exploration. During the optimization process, for

Table 6
Lower and upper limits used in the optimization of the PS model.

Parameters	Limits	
n_{CPU}	n_{CPU_l} 1	n_{CPU_u} 16
t_{RAM}	t_{RAM_l} 4	t_{RAM_u} 128
n_{DE}	n_{DE_l} 1	n_{DE_u} 8
n_{DS}	n_{DS_l} 1	n_{DS_u} 8
n_D	n_{D_l} 1	n_{D_u} 8

Table 7
Relevance factors and probabilities of occurrence for each type of connection in the PS model.

Type of connection	γ	$P(c)$
Process – CPU	S^a_{CPU}	$1/n_{CPU}$
Process – CPU queue	S^a_{CPU}	1
Process – RAM	S^a_R	$t_{RAM_{proc}}/t_{RAM}$
Process – RAM queue	S^a_R	1
Process – input device	S^a_{DE}	$1/n_{DE}$
Process – input device queue	S^a_{DE}	1
Process – output device	S^a_{DS}	$1/n_{DS}$
Process – output device queue	S^a_{DS}	1
Process – HD	S^a_D	$1/n_D$
Process – HD queue	S^a_D	1

each evaluated scenario, the metric components and the corresponding robustness values were calculated.

Performance was measured according to (14), with 100 replications performed for each scenario. The complexity was determined by calculating the sensitivity indices, taking into account each configuration, the probability of occurrence, and the relevance factors associated with each type of connection. The parameters of the PS model were adjusted within limits that reflect the processing and storage capacity of a typical computing system in the year 2024. The number of processing units ranged from 1 to 16, RAM varied from 4 MB to 128 MB, input devices ranged from 1 to 8, output devices from 1 to 8, and hard drives from 1 to 8.

The sensitivity indices for each scenario were calculated considering: (i) the parameter values of the scenario as reference values, (ii) the variation range of $[-90\%; 100\%]$ for the parameter values, restricted by the lower and upper limits specified in Table 6, and (iii) the analysis interval of $[-90\%; 100\%]$. The probabilities of occurrence $P(c)$ and the relevance factors γ for each type of connection in the model are provided in Table 7, where $S^a_{CPU}, S^a_{RAM}, S^a_{DE}, S^a_{DS}$ and S^a_D represent the sensitivity indices relative to the model parameters.

The six best scenarios, with the highest τ, were selected and recorded for c^β. The complexity of these scenarios was calculated based on the probabilities and relevance factors provided in Table 7. The complexity index for each scenario was calculated according to (4). The stability index for each scenario assessed during the optimization was calculated using (6). Table 8 displays the best swarms, resources, robustness index, performance, and complexity of the PS model after the optimization process. Each particle c^{a_i} in the swarm, with $i = 1, 2, \ldots, 15$, represented a distinct scenario. The values of the sensitivity, stability and complexity indices for the PS model in each scenario are presented in Table 9, where ID and OD refer to the input device and the output device, respectively.

5.2.2. Analysis of scenarios for the PS model

Analyzing Fig. 16, it is possible to observe that the x-axis represents the resource quantities for the eight scenarios with the highest robustness values found after the optimization process. The y-axis shows the

Table 8
Best swarms, resources, robustness index, performance, and complexity of the PS model.

c^{a_i}	CPU	RAM [MB]	ID	OD	HD	$\tau(c^{a_i})$	$\mu_d(c^{a_i})$	$\psi(c^{a_i})$
c^{a_9}	5	37	3	2	3	0.8965	0.7993	25.89
c^{a_3}	6	41	2	2	2	0.8956	0.8090	28.00
c^{a_8}	5	39	2	2	3	0.8952	0.8193	27.59
c^{a_1}	11	81	4	3	3	0.8887	0.8093	29.00
c^{a_6}	10	28	3	3	3	0.8877	0.8100	28.00
c^{a_2}	4	47	2	2	2	0.8858	0.8004	27.57

Table 9
Sensitivity, stability, and complexity indices for the PS model.

c^{a_i}	S^a_{CPU} [%]	S^a_{RAM} [%]	S^a_{DE} [%]	S^a_{DS} [%]	S^a_D [%]	$\xi(c^{a_i})$	$i_\psi(c^{a_i})$
c^{a_9}	25.98	32.52	3.14	31.25	6.11	0.9199	0.9702
c^{a_3}	25.98	33.52	3.14	31.25	6.11	0.9268	0.9509
c^{a_8}	17.75	22.71	25.30	0.53	33.71	0.8999	0.9664
c^{a_1}	8.07	23.39	17.53	46.87	4.14	0.9432	0.9135
c^{a_6}	15.87	5.72	13.56	17.36	47.49	0.9022	0.9510
c^{a_2}	2.38	20.91	35.10	5.49	36.12	0.8900	0.9668

performance values μ_d, the complexity index i_ψ, the stability index ξ and the robustness τ for each scenario.

Taking into account the quantitative analysis, the highest value of τ was observed for scenario (5, 37, 3, 2, 3), followed by scenarios (6, 41, 2, 2, 2), (5, 39, 2, 2, 3) and (11, 81, 4, 3, 3). The scenarios that succeeded c^β on the x-axis displayed similar τ values, with variations in μ_d, i_ψ, and ξ. Qualitative analysis showed that the highest μ_d was achieved when the model was simulated with c^β, effectively meeting the processing demand with the appropriate use of available computational resources. The μ_d values measured for scenarios with higher τ than the one recorded for c^β were slightly lower than the μ_d measured for c^β. In scenarios with high μ_d values, such as (5, 39, 2, 2, 3), (10, 28, 3, 3, 3), and (11, 81, 4, 3, 3): (i) resource idleness was low, (ii) process wait times in queues were reduced, and (iii) the ratio of generated to completed processes was high.

Further qualitative analysis shows that the highest value of i_ψ corresponds to c^β, since it serves as the reference index. The three scenarios with τ values higher than those recorded for c^β and with the highest i_ψ values are (5, 37, 3, 2, 3), (4, 47, 2, 2, 2), and (5, 39, 2, 2, 3). From a complexity perspective, one of the most important factors was the size of the queues for resource utilization, while from a performance perspective, the time processes spent in queues was one of the most significant factors.

In contrast to the values of μ_d and i_ψ, the ξ value for c^β was the lowest recorded. The highest value ξ was observed for the scenario (6, 30, 2, 2, 2). However, not only does this scenario not have a higher τ value compared to c^β, but it also has considerably lower values for μ_d and i_ψ than those of c^β. The scenarios with values τ higher than those recorded for c^β and with the highest values ξ are (11, 81, 4, 3, 3), (6, 41, 2, 2, 2) and (5, 37, 3, 2, 3). Considering both quantitative and qualitative analyses, the following scenarios are notable: (i) (11, 81, 4, 3, 3), which has the third highest μ_d value and the highest ξ value, being the fourth highest in τ, (ii) (5, 39, 2, 2, 3), which has the highest μ_d value and the third highest i_ψ value, being the third highest in τ, (iii) (6, 41, 2, 2, 2), which has the second highest ξ value, being the second highest in τ, and (iv) (5, 37, 3, 2, 3), which has the highest i_ψ and the third highest ξ value, being the highest in τ.

Analyzing the two scenarios with the highest τ values, it is evident that in the scenario (6, 41, 2, 2, 2), the values of μ_d and ξ were higher, while in the scenario (5, 37, 3, 2, 3), the value of i_ψ was higher. The final choice between the scenarios should be based on which metric components are considered most relevant in the analysis.

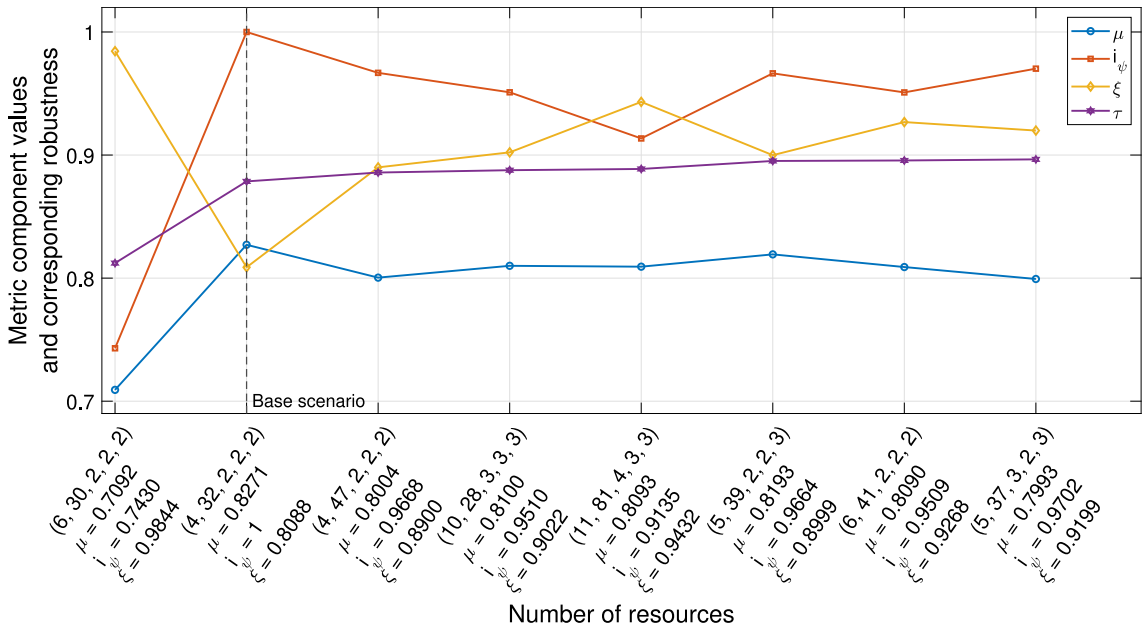

Fig. 16. Components of the metric and robustness × resource quantities for the PS model.

5.3. Determination of c^{β} and parameterization of the EVTB model

In the EVTB model, the base case was defined through consultation with experts in automotive engineering, who provided typical values for electric vehicle parameters. The configuration $c^{\beta} = (400, 75, 2)$ was selected to achieve the best performance in terms of average battery consumption and driving range, in economic driving mode with the electric motor active on the front axle and a driving cycle standardized by the New European Driving Cycle (NEDC) [108], derived from the Federal Test Procedure (FTP-75) [109].

Thus, when simulating the model with a 400 kWh battery, two electric motors rated at 75hp, an energy demand corresponding to three driving cycles, and a total distance of 53.5 km, the system objectives are met. In the context of the EVTB model, idleness refers to situations in which the battery level remains above 50% at the end of the route, while overload occurs when the battery level falls below 8% or when the energy supplied by the battery set is insufficient. Therefore, based on (15), the performance for c^{β} was calculated, resulting in $\mu_d = 0.9031$.

The urban driving cycle defined by the NEDC, which is derived from the FTP-75, consists of: (i) a cold-start transient phase, lasting 505 s, covering a distance of 5.8 km with an average speed of 41.2 km/h, (ii) a stabilized phase, lasting 866 s, covering a distance of 6.2 km with an average speed of 25.8 km/h (iii) a stop phase, lasting approximately 10 min, and (iv) a hot-start transient phase, lasting 505 s, covering a distance of 5.8 km with an average speed of 41.2 km/h. The maximum and average speeds in the cycle are 91.2 km/h and 34.1 km/h, respectively, and the minimum, average, and maximum accelerations are -1.5 m/s^2, 0 m/s^2, and 1.5 m/s^2, respectively.

The electric vehicle (EV) with a mass of 1580 kg, a height of 1565 mm, a width of 1790 mm and a length of 4480 mm was considered. The maximum cargo capacity of the electric vehicle was established at 415 kg. For the activation probabilities of each driving mode at any given time, the following values were adopted: 30% for the economic mode, 65% for the urban mode and 5% for the sport mode. The activation of each driving mode depends on the remaining battery level of the EV, with the economic mode available at any time, the urban mode available only when the battery level is above 10%, and the sport mode available only when the battery level is above 50%. The power ratings considered for the DC/AC and AC/DC inverters of the electric vehicle were 87 kW and 48 kW, respectively.

The reference minimum range a_{ref} adopted was 450 km. The battery level defined for the electric vehicle at the beginning of each simulation was 100%. To calculate the resistive forces acting on the EV in each simulation instant, the following were considered: the standard acceleration due to gravity 9.81 m/s^2, the sum of the masses of the EV and its maximum cargo capacity 1995 kg, a fixed tire diameter of 647 mm, a fixed frontal area of 2.8 m^2, and a variation of the inclination of the pavement (in degrees) following a uniform distribution $U(0,\ 10)$. Concerning atmospheric factors, 1.22 kg/m^3 was used for air density [110], and an average wind speed of 4.5 m/s was adopted. In the simulations, a value of 0.23 was used for the aerodynamic drag coefficient, considering an EV with a hatchback body type [111]. The same settings for the EVTB model were maintained in all simulations performed.

5.3.1. Application of the robustness metric in the EVTB model

In assessing the robustness of the EVTB model using the proposed metric, aspects related to the design and operation of the modeled electric vehicle (EV) were examined. From a design point of view, the accuracy of battery power size p_B, electric machine power p_M, and the number of electric machines n_M was analyzed. From an operational perspective, the analysis allowed for the evaluation of robustness behavior as parameter values varied. The variation in robustness is related to: (i) battery consumption and EV range, (ii) connections made during EV operation, and (iii) the ability to maintain balance when EV characteristics are altered. To identify scenarios with robustness values higher than those calculated for c^{β}, an optimization process was carried out using the particle swarm optimization algorithm (PSO) with a swarm of 15 particles, considering (12) as the evaluation function. The lower and upper bounds used for the parameter values in the optimization were given by:

$$M_{lim} = \begin{bmatrix} p_{B_l} & p_{B_u} \\ p_{M_l} & p_{M_u} \\ n_{M_l} & n_{M_u} \end{bmatrix} \tag{19}$$

where p_{B_l} and p_{B_u} denote the lower and upper bounds of p_B, p_{M_l} and p_{M_u} denote the lower and upper bounds of p_M, and n_{M_l} and n_{M_u} denote the lower and upper bounds of n_M. These bounds are listed in Table 10, where the subscript $_l$ represents the lower bound and $_u$ represents the upper bound.

Table 10
Lower and upper limits used in the optimization of the EVTB model.

Parameters	Limits	
p_B	p_{B_l} 100	p_{B_u} 1000
p_M	p_{M_l} 37.5	p_{M_u} 180
n_M	n_{M_l} 1	n_{M_u} 4

Table 11
Probabilities of connection occurrence in traction and braking states.

State	$P(c)$
Traction	0.5
Braking	0.5

The stopping criteria for the optimization process were defined by the maximum number of iterations, $n_{iter} = 50$, or by achieving an evaluation function value below $f_{aval} < 10^{-6}$. For the inertia coefficient w, the values $w_{max} = 1.2$ and $w_{min} = 0.9$ were adopted. The particle acceleration coefficients were established at $c_1 = c_2 = 2.0$. The parameters of the EVTB model were adjusted within ranges that reflect the technical specifications of electric vehicles available on the market in 2024. The battery power ranged from 20 kW to 100 kW, the electric motor power from 10 kW to 50 kW, and the number of electric motors from 1 to 4, covering the economic, urban and sport driving modes.

Each component of the metric was calculated during the optimization process, allowing the robustness value to be determined for each evaluated scenario. The performance of each scenario was calculated on the basis of (15). Each simulation consisted of 100 replications. To ensure that the second term in the numerator of expression (15) is greater than or equal to 1, the following conditions were adopted:

$$a_r = \begin{cases} a_r & if \quad a_r \leq a_{ref} \\ a_{ref} & if \quad a_r > a_{ref} \end{cases} \tag{20}$$

To calculate the complexity of the scenarios evaluated during optimization, it was necessary to obtain sensitivity indices for each scenario, considering the probabilities of occurrence for each type of connection and their respective relevance factors. The sensitivity indices for each scenario were calculated based on: (i) the values of the scenario parameters as reference values, (ii) a variation range of $[-90\%; 100\%]$ for the values of the model parameters, restricted by the lower and upper bounds listed in Table 10, and (iii) an analysis interval of $[-90\%; 100\%]$. The probabilities of connection occurrence $P(c)$ when EVTB states are provided in Table 11. Since only traction and braking states occur during the operation of the electric vehicle, the probability that the model is in either of these states is 50%. Therefore, all connections between elements involved in vehicle traction (shown in blue in Fig. 12) have the same probability of occurring. The same reasoning applies to the elements involved in the braking process (shown in red in Fig. 12).

Table 12 presents the relevance factors γ for each type of connection in the model, where S^a_B, S^a_M and S^a_{NM} are the sensitivity indices related to the model parameters. Control connections require the entire modeled system to be operational, therefore, they are influenced by all parameters and have a relevance factor of *one*. CC and CA connections are influenced by the electrical power provided by the battery. Torque transfer connections are affected by both the mechanical power provided by the electric machine and the number of electric motors. The complexity of the scenarios was calculated considering the probabilities listed in Table 11, weighted by the relevance factors given in Table 12. The complexity index for each scenario was calculated using (4). The stability indices for each scenario evaluated during optimization were calculated using (6).

Table 12
Relevance factors for each type of connection in the EVTB model.

Type of connection	γ
Control	$S^a_B + S^a_M + S^a_{NM}$
DC and AC	S^a_B
Torque	$S^a_M + S^a_{NM}$

Table 13
Best swarms, resources, robustness index, performance, and complexity of the EVTB model.

c^{a_i}	B [kWh]	M [hp]	NM	$\tau(c^{a_i})$	$\mu_d(c^{a_i})$	$\psi(c^{a_i})$
$c^{a_{12}}$	670	175	2	0.9261	0.8722	12.47
c^{a_3}	331	121	2	0.9085	0.8754	13.10
$c^{a_{14}}$	729	173	2	0.9018	0.9022	13.37
c^{a_7}	607	115	4	0.8969	0.8827	13.60
$c^{a_{13}}$	462	142	2	0.8500	0.8932	13.98

Table 14
Sensitivity, stability, and complexity indices for the EVTB model.

c^{a_i}	S^a_B [%]	S^a_M [%]	S^a_{NM} [%]	$\xi(c^{a_i})$	$i_\psi(c^{a_i})$
$c^{a_{12}}$	18.80	63.42	17.78	0.9437	0.9623
c^{a_3}	50.89	45.76	3.35	0.9399	0.9102
$c^{a_{14}}$	11.09	62.15	26.76	0.9154	0.8877
c^{a_7}	8.93	30.21	60.86	0.9402	0.8679
$c^{a_{13}}$	51.84	3.29	44.87	0.8200	0.8367

Among the various simulations, the five best were selected based on robustness. Table 13 presents the best swarms, resources, robustness, performance, and complexity indices of the EVTB model obtained after the optimization process. Each particle c^{a_i} in the swarm, with $i = 1, 2, \ldots, 15$, represents a distinct scenario. The sensitivity, stability, and complexity indices for the EVTB model for each scenario are listed in Table 14. Two scenarios were found with τ greater than the value recorded for c^β. In Table 13, **B** denotes the electrical power supplied by the battery, **M** denotes the mechanical power provided by the electric machine, and **NM** denotes the number of electric machines.

5.3.2. Analysis of scenarios for the EVTB model

Fig. 17 shows the resource quantities for the eight scenarios with the highest robustness values identified after the optimization process on the x-axis. The y-axis displays the performance values μ_d, the complexity index i_ψ, the stability index ξ and the robustness τ for each scenario. From a quantitative perspective, only two scenarios have τ greater than c^β: (670, 175, 2) and (331, 121, 2). However, scenarios (729, 173, 2) and (607, 115, 4), which are near c^β, exhibit satisfactory τ values. There is a noticeable proximity between the values of τ of scenarios close to c^β, with variations in μ_d, i_ψ and ξ. Therefore, a qualitative analysis is conducted.

From the qualitative analysis, it was observed that the μ_d value for c^β was the highest obtained. In this scenario, the electric vehicle can complete the proposed route using the charge of the battery pack effectively, meeting the travel demand. The two scenarios with the highest values of τ have values of μ_d lower than those calculated for c^β. However, the following scenarios with values τ close to c^β recorded satisfactory μ_d values: (729, 173, 2), (462, 142, 2) and (490, 128, 2). In these scenarios with satisfactory μ_d values: (i) the average battery consumption of the EV during the route approached the maximum recorded consumption, indicating less variation in battery consumption and (ii) the remaining autonomy and the minimum reference autonomy were closer, reflecting the efficiency of battery pack sizing considering the traveled route.

In the qualitative analysis, the highest value i_ψ was observed for c^β, since this scenario serves as reference for the index. Including c^β, the two scenarios with the highest values of τ also exhibited the highest values of i_ψ. Although the scenario (729, 173, 2) did not have a τ value

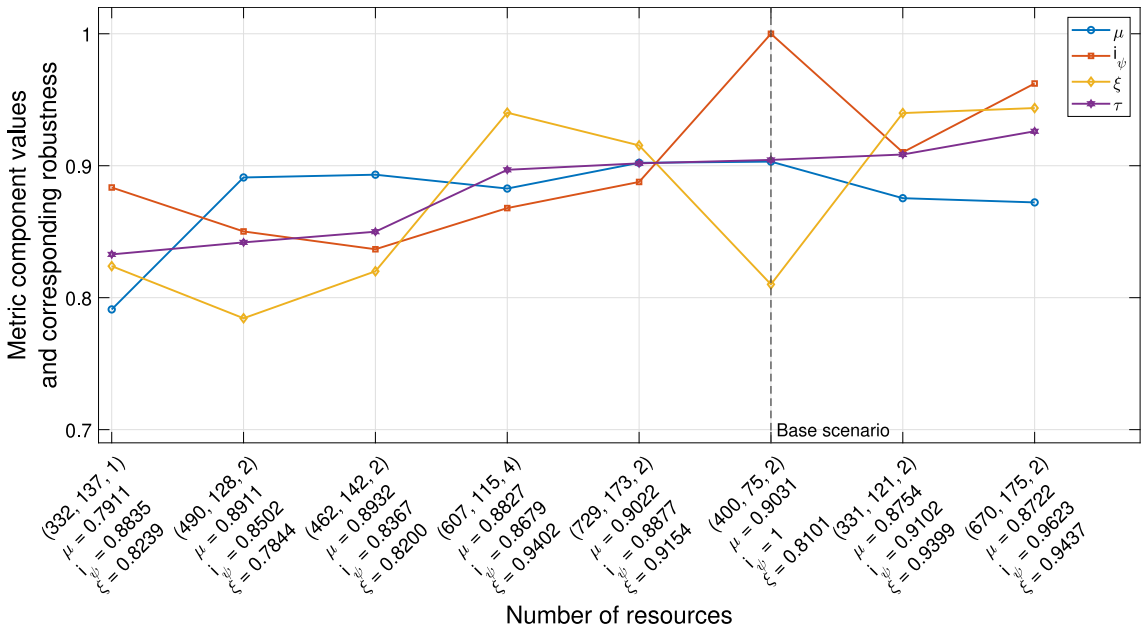

Fig. 17. Components of the metric and robustness × resource quantity for the EVTB model.

greater than c^β, it had the third highest i_ψ value. In contrast to μ_d and i_ψ, the value of ξ for c^β was not the highest, being the second lowest recorded. Scenarios with τ values higher than c^β had the highest and third highest ξ values, respectively. The scenario (607, 115, 4), although it did not have a value of τ greater than c^β, had the second highest value of ξ.

Based on quantitative and qualitative analyses, it is observed that: (i) scenario (331, 121, 2) exhibited the second highest value i_ψ and the third highest value ξ, with the second highest τ value and (ii) the scenario (670, 175, 2) had the highest values i_ψ and ξ and also the highest value τ. The final criterion for choosing between scenarios should be the relevance assigned to each component of the metric in the analysis.

In a general analysis, the values of the three components of the robustness metric contribute differently to the τ value. To determine the contribution of performance to the robustness value, (21) should be used. To determine the contributions of the complexity index and the stability index to the robustness value, the numerator in (21) should be replaced by i_ψ or ξ, respectively, as:

$$\frac{\mu_d}{\mu_d + i_\psi + \xi} \tag{21}$$

Analyzing Fig. 18, the percentage contribution of each component of the metric to the value τ can be observed for the scenarios listed in Tables 3 and 4, 8 and 9, 13 and 14. Taking into account Figs. 18(a), 18(b), and 18(c), which correspond to the ICU, PS, and EVTB models, respectively, it is observed that in these robustness scenarios, the contributions of the components to the value τ are approximately equal. Specifically, the contribution of $\mu_d \approx 30\%$, while the contributions of i_ψ and $\xi \approx 35\%$.

The intervals between the values of μ_d, i_ψ, and ξ for c^β and the values near them can be used as radii to define regions of interest for analysis. For example, the interval between the ξ value for c^β and the highest ξ value observed in the scenarios analyzed can define a region containing ξ values indicative of robust solutions. Thus, scenarios located at the intersection of regions of interest related to μ_d, i_ψ, and ξ constitute the robustness region. Therefore, scenarios exhibiting greater robustness than the base scenario are included in the robustness region.

As the values of τ decrease, the contribution of i_ψ to the value of τ tends to decrease, while the contributions of μ_d and ξ tend to increase in the ICU and PS models, with ξ showing a higher contribution. In the EVTB model, the contribution of i_ψ to the value τ increases in scenarios close to the robustness region and continues to increase in scenarios further from this region. This behavior is attributed to the decrease in performance and stability index in scenarios with lower associated robustness, along with the fact that these scenarios have complexity indices close to *one*.

5.4. Discussion

This work developed a multidimensional robustness metric that integrates performance, complexity, and stability, enabling a comprehensive and detailed analysis of various scenarios in discrete models. The proposed approach was applied to three distinct models: an intensive care unit (ICU) system, a process scheduling (PS) model, and an electric vehicle traction and braking (EVTB) model. The robustness metric effectively identified robust scenarios by considering the system's ability to maintain performance and stability under parameter variations, providing a valuable tool for analyzing and optimizing complex systems.

The sensitivity of the systems with respect to the robustness indicator was evaluated by sensitivity analysis. Specifically, in the ICU model, the analysis indicated that the patient arrival rate and the rate of adverse events had a significant impact on system performance and stability. In the PS model, the most sensitive parameters were the amount of RAM and the number of processing units, directly affecting processing time and resource utilization. In the EVTB model, battery power and number of motors were identified as the most critical factors that influence vehicle range and energy consumption. These findings were instrumental in identifying the most robust scenarios for each model. In summary, the analyses highlighted the parameters with the greatest influence on robustness, providing valuable input for system adjustment and optimization.

The best results were achieved in scenarios where performance was slightly lower than baseline, but stability was significantly higher. These scenarios, located within the robustness region, demonstrated efficiency in maintaining system functionality even under adverse conditions. Specifically, in the ICU model, the scenario (13, 122, 97, 11, 35) emerged as the most robust, balancing performance and stability. In the PS model, scenario (5, 37, 3, 2, 3) exhibited the highest robustness index, while in the EVTB model, scenario (670, 175, 2) showed the highest robustness.

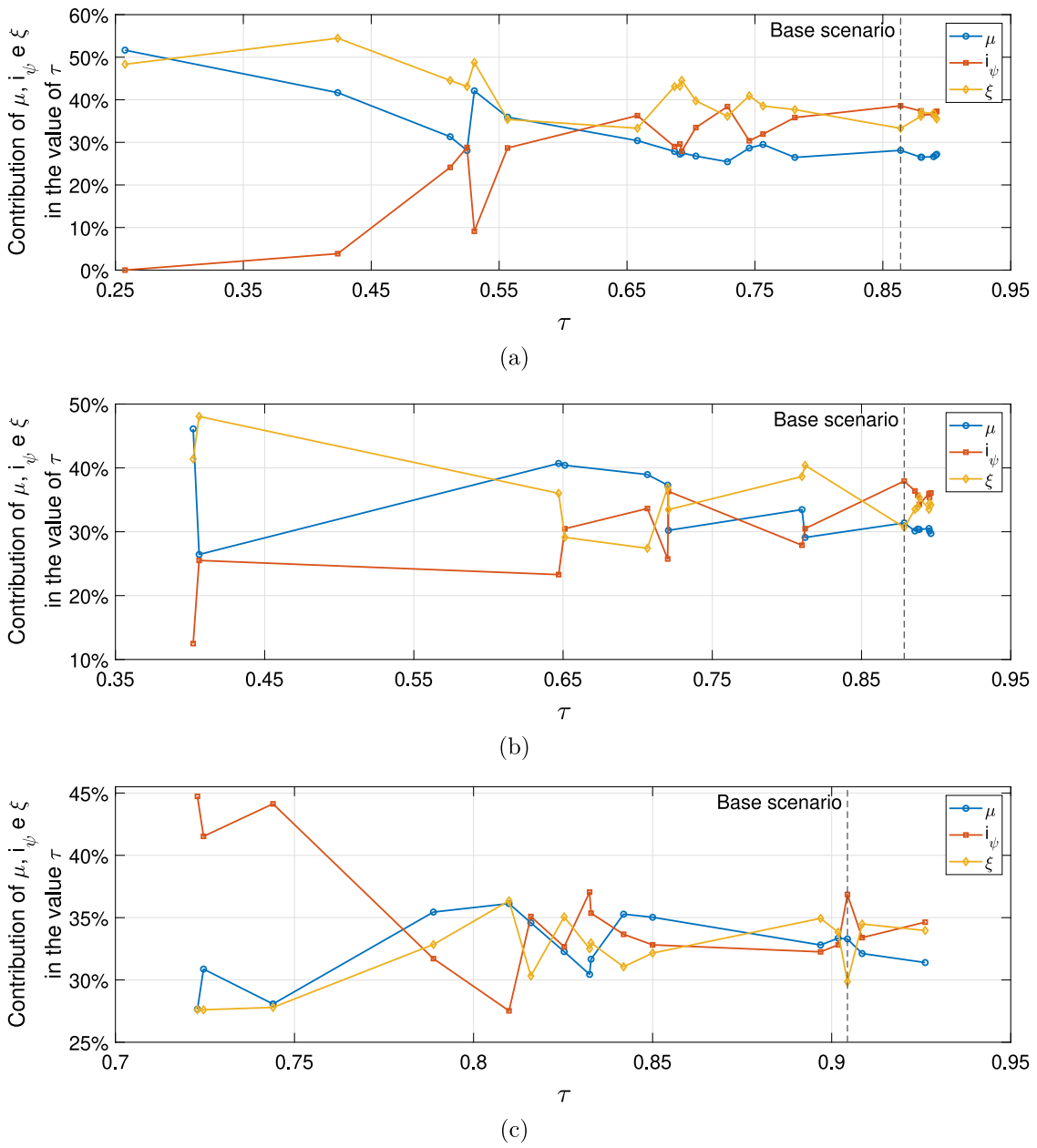

Fig. 18. Contribution in [%] of μ_d, i_ψ, and ξ to the value of τ for: (a) ICU model, (b) PS model and (c) EVTB model.

The results align with previous studies in the literature that emphasize the importance of considering multiple dimensions when evaluating the robustness of the system. The research by Mitchell [15] and Holland [14] has already highlighted complexity and emergence as critical factors in the evaluation of complex systems. The proposed metric supports this perspective by integrating various aspects of the system, enabling a more comprehensive and well-founded analysis. In addition, the findings reinforce the notion that robust scenarios are not necessarily those with the best isolated performance, but rather those that maintain a balance between performance, complexity, and stability [112].

However, some results differ from traditional approaches that prioritize maximum performance as the primary optimization criterion. In models where stability and complexity are not considered, focus solely on performance can lead to the selection of scenarios that, although efficient under normal conditions, do not maintain robustness when faced with disturbances or changes in the operational environment [113,114]. This study demonstrates that by integrating robustness with other dimensions, potential failures that would not be identified in a performance-only analysis can be avoided.

The comparison among the three case studies demonstrates both the flexibility and consistency of the proposed method. In all models, ICU, PS and EVTB, the robustness metric was able to capture significant variations in input parameters, coherently reflecting their impacts on performance, complexity and stability. Although systems differ in nature (healthcare, computational and automotive), a common pattern was observed: Robustness tends to increase in configurations with lower relative complexity and greater stability, provided that performance remains within acceptable operational limits.

Even so, each system exhibited specific sensitivities. In the ICU model, external factors, such as patient arrival rate and adverse events, were the most influential. In the PS model, internal hardware resources, namely RAM and CPU, had the greatest impact. In the EVTB model, robustness was strongly associated with the energy configuration, particularly battery power and the number of motors. These differences demonstrate that, although the method is applicable in

diverse contexts, its effectiveness depends on the proper identification and characterization of the most relevant parameters in each domain, which reinforces the importance of the integrated approach proposed in this study.

The main gap identified in the literature is the lack of a unified metric that efficiently integrates the dimensions of performance, complexity, and stability. This work addresses this gap by proposing a metric that can be applied across different contexts, providing a more comprehensive approach to the analysis of complex systems. Furthermore, the methodology used can be extended to other types of system, including those with continuous variables, suggesting new avenues for future research.

The primary challenges encountered during this work were the extensive time required for simulations and the limited information available about the systems, particularly in the PS model and the EVTB model. However, the use of parallel computing helped mitigate the issue of simulation time, and expert consultations, along with a thorough review of the literature, were important in accurately parameterizing the models. Any errors in the modeling process were addressed by successive simulations and iterative adjustments.

Considering the challenges encountered throughout this study, it is important to acknowledge certain limitations of the proposed method, particularly its application to simulatable models. In such cases, the metric depends on the availability of validated models and the precise definition of parameters related to performance, complexity, and stability. In real-world systems, on the contrary, the metric can be applied directly, provided that variable values are continuously monitored or through sampling. Simplified representations are only necessary when reliable data or adequate models are not available. However, when robustness is calculated directly in real systems, the computational effort required for sensitivity analysis and the optimization process tends to increase significantly with the dimensionality of the search space. Therefore, future research should explore strategies to reduce computational complexity in these scenarios and evaluate the applicability of the method in models with limited data availability or nonsimulatable dynamics.

These considerations open new perspectives for the use of the metric in operational systems, where robustness can be monitored over time to support strategic decision making. Potential application domains include financial systems, platforms for tracking socioeconomic indicators (such as the Human Development Index and Gross Domestic Product), and other complex environments subject to external fluctuations and multiple sources of uncertainty. In such contexts, the metric can contribute to early detection of vulnerabilities and adjustment of operational parameters based on resilience and stability criteria.

6. Conclusion

This study was based on the hypothesis that, if performance, complexity, and stability can be measured consistently, it would be feasible to integrate these dimensions into a unified robustness metric. To investigate this hypothesis, a method was proposed that enables the calculation of robustness through the weighted combination of these three indicators. The metric was validated using three distinct models: an Intensive Care Unit (ICU) system, a Process Scheduling (PS) model, and an Electric Vehicle Traction and Braking (EVTB) system, each presenting different operational and structural characteristics.

The application of the metric revealed that robustness is enhanced by solutions that combine performance efficiency, low complexity, and stability under varying operational conditions. Each system demonstrated sensitivity to specific parameters: in the ICU model, patient arrival rate and adverse event rate; in the PS model, the amount of RAM and the number of CPUs; and in the EVTB model, the battery power and the number of electric motors.

The analysis reinforced the importance of addressing performance, complexity, and stability in an integrated way, providing a tool capable of evaluating and optimizing the resilience of complex systems. Therefore, it is concluded that the proposed metric can effectively represent robustness across different systems, supporting the identification of resilient solutions and enhancing decision making in diverse operational environments.

As a natural extension of this work, the proposed metric can be applied to other domains, such as logistics systems, power grids, and industrial processes. Furthermore, integrating the method with machine learning techniques could further enhance its potential, particularly in tasks such as automatic hyperparameter optimization and the identification of operational patterns related to robustness. These extensions may strengthen the predictive and adaptive capabilities of the model, contributing to the development of more resilient systems in uncertain and dynamic environments.

CRediT authorship contribution statement

João Ricardo B. Paiva: Writing – review & editing, Writing – original draft, Visualization, Validation, Supervision, Software, Resources, Methodology, Investigation, Formal analysis, Data curation, Conceptualization. **Viviane M. Gomes Pacheco:** Visualization, Validation, Software, Methodology, Investigation, Formal analysis, Data curation. **Júnio Santos Bulhões:** Writing – review & editing, Writing – original draft, Visualization, Software, Resources. **Clóves Gonçalves Rodrigues:** Writing – review & editing, Writing – original draft, Visualization, Software, Resources. **António Paulo Coimbra:** Writing – review & editing, Writing – original draft, Visualization, Software, Resources. **Wesley Pacheco Calixto:** Writing – review & editing, Writing – original draft, Visualization, Validation, Supervision, Software, Resources, Project administration, Methodology, Investigation, Formal analysis, Data curation, Conceptualization.

Declaration of competing interest

The authors declare that they have no financial interests or conflicts of interest that could potentially influence the objectivity, integrity, or impartiality of our research findings. Specifically:

1. Financial Support: The research conducted and the preparation of this manuscript received no external financial support, grants, or funding from any public or private entity.

2. Patents: We confirm that there are no patents associated with the research work presented in this manuscript, and no patent applications have been submitted during the course of this study.

3. Salary Reimbursement: The authors involved in this research project have not received any salary, fees, or reimbursements related to the publication of this work. The research was conducted as part of our academic and professional activities, and no financial compensation has been sought or received.

Acknowledgments

The authors acknowledge the financial support provided by the Fundação para a Ciência e a Tecnologia (FCT/Portugal), I.P., under project UIDB/00048/2020 (DOI: 10.54499/UIDB/00048/2020), and the National Council for Scientific and Technological Development (CNPq/Brazil) through a Research Productivity Fellowship (Grant No. 301644/2022-5). Furthermore, the authors express their gratitude to the Coordination for the Improvement of Higher Education Personnel (CAPES/Brazil) for the postdoctoral fellowship (Grant No. 88887.985910/2024-00). The authors also thank LaMCAD/UFG for providing the computational resources that supported this research.

Data availability

Data will be made available on request.

References

[1] D.R. Ilgen, J. Schneider, Performance measurement: A multi-discipline view, Int. Rev. Ind. Organ. Psychol. 6 (1991) 71–108.
[2] W.C. Borman, D.H. Brush, More progress toward a taxonomy of managerial performance requirements, Hum. Perform. 6 (1) (1993) 1–21.
[3] J.P. Campbell, R.A. McCloy, S.H. Oppler, C.E. Sager, A theory of performance, Pers. Sel. Organ. 3570 (1993) 35–70.
[4] J.P. Campbell, The definition and measurement of performance in the new age, in: Pulakos (Ed.), The Changing Nature of Performance: Implications for Staffing, Motivation, and Development, vol. 399, 1999, p. 429.
[5] C.M. Cadwell, Performance Management, AMACOM Div American Mgmt Assn, 2002.
[6] H.A. Simon, The architecture of complexity, Proc. Am. Phil. Soc. 106 (6) (1962) 467–482.
[7] P. Bak, K. Wiesenfeld, Self-organized criticality: and explanation of 1/f noise, Phys. Rev. Lett. 59 (1987) 381–384.
[8] H.A. Simon, Models of My Life, MIT Press, 1991.
[9] J.M. Sussman, Ideas on complexity in systems–twenty views, 2000, p. 2008, Retrieved October 3.
[10] S. Lloyd, Measures of complexity: a nonexhaustive list, IEEE Control Syst. Mag. 21 (4) (2001) 7–8.
[11] Y. Bar-Yam, Complexity rising: From human beings to human civilization, a complexity profile, in: Encyclopedia of Life Support Systems, EOLSS, UNESCO, EOLSS Publishers, Oxford, UK, 2002.
[12] J.M. Ottino, Engineering complex systems, Nature 427 (6973) (2004) 399.
[13] W. Meed, Complexity science and the social world, in: K. Kempf-Leonard (Ed.), Encyclopedia of Social Measurement, Elsevier, Salford, Greater Manchester, United Kingdom, 2005, pp. 399–403.
[14] J.H. Holland, Studying complex adaptive systems, J. Syst. Sci. Complex. 19 (1) (2006) 1–8.
[15] M. Mitchell, Complexity: A Guided Tour, first ed., Oxford University Press, Oxford, United Kingdom 2009, ISBN: 9780199798100, 2009.
[16] G.E. Mobus, M.C. Kalton, et al., Principles of Systems Science, vol. 7, Springer, 2015, 5.
[17] O.A. Rosso, L.C. Carpi, P.M. Saco, M.G. Ravetti, A. Plastino, H.A. Larrondo, Causality and the entropy–complexity plane: Robustness and missing ordinal patterns, Phys. A 391 (1) (2012) 42–55, http://dx.doi.org/10.1016/j.physa.2011.07.030.
[18] M. Batty, R. Morphet, P. Masucci, K. Stanilov, Entropy, complexity, and spatial information, J. Geogr. Syst. 16 (4) (2014) 363–385, http://dx.doi.org/10.1007/s10109-014-0202-2.
[19] D.P. Feldman, J.P. Crutchfield, Measures of statistical complexity: Why? Phys. Lett. A 238 (4–5) (1998) 244–252, http://dx.doi.org/10.1016/S0375-9601(97)00855-4.
[20] S.A. Abdallah, M.D. Plumbley, A measure of statistical complexity based on predictive information with application to finite spin systems, Phys. Lett. A 376 (4) (2012) 275–281, http://dx.doi.org/10.1016/j.physleta.2011.10.066.
[21] A. Arbona, C. Bona, B. Miñano, A. Plastino, Statistical complexity measures as telltale of relevant scales in emergent dynamics of spatial systems, Phys. A 410 (2014) 1–8.
[22] J.D. Corbit, D.J. Garbary, Fractal dimension as a quantitative measure of complexity in plant development, Proc. R. Soc. Lond. [Biol] 262 (1363) (1995) 1–6.
[23] G. Young, S. Dey, A. Rogers, D. Exton, Cost and time-effective method for multi-scale measures of rugosity, fractal dimension, and vector dispersion from coral reef 3D models, PLoS One 12 (4) (2017).
[24] M. Gell-Mann, S. Lloyd, Information measures, effective complexity, and total information, Complexity 2 (1) (1996) 44–52, http://dx.doi.org/10.1002/(SICI)1099-0526(199609/10)2:1%3C44::AID-CPLX10%3E3.0.CO;2-X.
[25] N. Ay, M. Muller, A. Szkola, Effective complexity and its relation to logical depth, IEEE Trans. Inform. Theory 56 (9) (2010) 4593–4607, http://dx.doi.org/10.1109/TIT.2010.2053892.
[26] T. Deacon, S. Koutroufinis, Complexity and dynamical depth, Information 5 (3) (2014) 404–423, http://dx.doi.org/10.3390/info5030404.
[27] H. Koorehdavoudi, P. Bogdan, A statistical physics characterization of the complex systems dynamics: quantifying complexity from spatio-temporal interactions, Sci. Rep. 6 (2016) 27602.
[28] V.M. Gomes, J.R. Paiva, M.R. Reis, G.A. Wainer, W.P. Calixto, Mechanism for measuring system complexity applying sensitivity analysis, Complexity 2019 (2019).
[29] A. Paice, F. Wirth, Analysis of the local robustness of stability for maps, in: Control Conference (ECC), 1997 European, IEEE, 1997, pp. 1259–1264.
[30] Y. Okuyama, Stability analysis of discrete event systems using multiple metrics and simultaneous linear inequalities, in: 2016 55th Annual Conference of the Society of Instrument and Control Engineers of Japan, SICE, IEEE, 2016, pp. 1141–1146.
[31] A. Pesterev, Absolute stability analysis for a linear time varying system of special form, in: 2016 International Conference Stability and Oscillations of Nonlinear Control Systems, Pyatnitskiy's Conference, IEEE, 2016, pp. 1–3.
[32] V. Chestnov, D. Shatov, Modified circle criterion of absolute stability and robustness estimation, in: 2018 14th International Conference Stability and Oscillations of Nonlinear Control Systems (Pyatnitskiy's Conference), STAB, IEEE, 2018, pp. 1–4.
[33] Z. Liu, X. He, Z. Ding, Z. Zhang, A basin stability based metric for ranking the transient stability of generators, IEEE Trans. Ind. Inform. 15 (3) (2019) 1450–1459.
[34] X. Zhong, E. Santos, R. McCartney, Exploring the relationship between knowledge and algorithm performance in discrete optimization, in: 16th IEEE International Conference on Tools with Artificial Intelligence, IEEE, 2004, pp. 604–611.
[35] L. Wan, J. Luo, On the complexity of wireless multicast optimization, IEEE Wirel. Commun. Lett. 1 (6) (2012) 593–596.
[36] P. Laddha, S.P. Ramalingam, Bitrate and complexity optimizations for video conferencing systems, in: 2016 IEEE International Conference on Consumer Electronics, ICCE, IEEE, 2016, pp. 235–236.
[37] O. Hammami, System theoretical complexity (STC): On the benefits of system multiobjective optimization and automatic model composition, in: 2018 IEEE International Systems Engineering Symposium, ISSE, IEEE, 2018, pp. 1–7.
[38] K. Krishnaswamy, G. Papageorgiou, S. Glavaski, A. Papachristodoulou, Analysis of aircraft pitch axis stability augmentation system using sum of squares optimization, in: Proceedings of the 2005, American Control Conference, 2005, IEEE, 2005, pp. 1497–1502.
[39] W.-J. Shyr, C.-H. Hsu, C.-H. Chen, C.-F. Wu, Robust stability analysis of discrete time system via an optimization approach, in: Second International Conference on Innovative Computing, Information and Control, ICICIC 2007, IEEE, 2007, 103–103.
[40] A. Keshtkar, H. Bolandi, A.A. Jalali, Design and optimization of robust PID controller via stability methods for a class of uncertainty systems, in: 2007 Mediterranean Conference on Control & Automation, IEEE, 2007, pp. 1–5.
[41] M. Odintsov, K. Gerasimenko, D. Akimov, Application of multiobjective optimization methods for improving of power system static stability, in: 2015 IEEE NW Russia Young Researchers in Electrical and Electronic Engineering Conference, EIConRusNW, IEEE, 2015, pp. 251–253.
[42] I. Nassar, I. Elsayed, M. Abdella, Optimization and stability analysis of offshore hybrid renewable energy systems, in: 2019 21st International Middle East Power Systems Conference, MEPCON, IEEE, 2019, pp. 583–588.
[43] A. Tolk, Simulation-based optimization: Implications of complex adaptive systems and deep uncertainty, Information (ISSN: 2078-2489) (10) (2022) 469, http://dx.doi.org/10.3390/info13100469.
[44] A. Vasudeva, N.A. Sheikh, Making sense of complexity: Our era most important challenge, J. Fam. Med. Prim. Care (ISSN: 2249-4863) 12 (4) (2023) 801–802, http://dx.doi.org/10.4103/jfmpc.jfmpc_168_23.
[45] M. Rostami, S. Bucking, A framework for integrating reliability, robustness, resilience, and vulnerability to assess system adaptivity, in: Volume 13: Safety Engineering, Risk, and Reliability Analysis; Research Posters, American Society of Mechanical Engineers, 2021, http://dx.doi.org/10.1115/imece2021-73021.
[46] P. Okoh, S. Haugen, Improving the robustness and resilience properties of maintenance, Process. Saf. Environ. Prot. 94 (2015) 212–226.
[47] S. Wang, X. Gu, J. Chen, C. Chen, X. Huang, Robustness improvement strategy of cyber-physical systems with weak interdependency, Reliab. Eng. Syst. Saf. 229 (2023) 108837.
[48] R.D. Stacey, Strategic Management and Organisational Dynamics: The Challenge of Complexity to Ways of Thinking About Organisations, sixth ed., Prentice Hall, 2011.
[49] J.R. Paiva, V.M. Gomes, M.R. Reis, G. Wainer, W.P. Calixto, Relationship between risk and complexity in system using connection based metric, in: 2018 IEEE International Conference on Environment and Electrical Engineering and 2018 IEEE Industrial and Commercial Power Systems Europe, EEEIC / I&CPS Europe, 2018, pp. 1–5.
[50] G.C. Critchfield, K.E. Willard, D.P. Connelly, Probabilistic sensitivity analysis methods for general decision models, Comput. Biomed. Res. 19 (3) (1986) 254–265.
[51] A. Saltelli, S. Tarantola, F. Campolongo, M. Ratto, Sensitivity Analysis in Practice: a Guide to Assessing Scientific Models, John Wiley & Sons, 2004.
[52] T. Homma, A. Saltelli, Importance measures in global sensitivity analysis of nonlinear models, Reliab. Eng. Syst. Saf. 52 (1) (1996) 1–17.
[53] D.J. Pannell, Sensitivity analysis: strategies, methods, concepts, examples, Agric. Econ. 16 (1997) 139–152.
[54] C. Frey, S.R. Patil, Identification and review of sensitivity analysis methods, Risk Anal. 22 (3) (2002) 553–578.
[55] D. Hamby, A comparison of sensitivity analysis techniques, Health Phys. 68 (2) (1995) 195–204.
[56] A. Saltelli, S. Tarantola, K.-S. Chan, A quantitative model-independent method for global sensitivity analysis of model output, Technometrics 41 (1) (1999) 39–56.
[57] D. Hamby, A review of techniques for parameter sensitivity analysis of environmental models, Environ. Monit. Assess. 32 (2) (1994) 135–154.
[58] T.M. Romanowicz, Structural sensitivity analysis in a certain class of linear systems, IEEE Trans. Syst. Man Cybern. (3) (1983) 413–417.

[59] F.H. Clarke, P.D. Loewen, Sensitivity analysis in optimal control, in: Decision and Control, 1984. the 23rd IEEE Conference on, IEEE, 1984, pp. 1649–1654.
[60] N.H. Kim, H. Wang, N.V. Queipo, Adaptive reduction of random variables using global sensitivity in reliability-based optimisation, Int. J. Reliab. Saf. 1 (1–2) (2006) 102–119.
[61] T.G. Eschenbach, L.S. McKeague, Exposition on using graphs for sensitivity analysis, Eng. Econ. 34 (4) (1989) 315–333.
[62] S.H. Fetsch, N.O. DeBasio, Academic service partnerships: Organizational efficiency and efficacy between organizations, J. Prof. Nurs. 27 (6) (2011) e82–e89.
[63] K.-H. Chang, Improving the efficiency and efficacy of stochastic trust-region response-surface method for simulation optimization, IEEE Trans. Autom. Control 60 (5) (2014) 1235–1243.
[64] D. Oliveira, P. Navaux, P. Rech, Increasing the efficiency and efficacy of selective-hardening for parallel applications, in: 2019 IEEE International Symposium on Defect and Fault Tolerance in VLSI and Nanotechnology Systems, DFT, IEEE, 2019, pp. 1–6.
[65] S.E. Page, Diversity and Complexity, Princeton University Press, 2010.
[66] J.H. Holland, Complexity: A Very Short Introduction, Oxford University Press, 2014.
[67] J.L. Casti, Complexification: Explaining a paradoxical world through the science of surprise, 1995.
[68] Y. Bar-Yam, Dynamics of Complex Systems, first ed., vol. 213, Addison-Wesley, Newton, Massachusetts, USA, ISBN: 9780813341217, 1997.
[69] M. Gell-Mann, Simplicity and complexity in the description of nature, Eng. Sci. 51 (3) (1988) 2–9.
[70] C. Gershenson, N. Fernández, Complexity and information: Measuring emergence, self-organization, and homeostasis at multiple scales, Complexity 18 (2) (2012) 29–44.
[71] F.C. Santos, F.L. Pinheiro, T. Lenaerts, J.M. Pacheco, The role of diversity in the evolution of cooperation, J. Theoret. Biol. 299 (2012) 88–96.
[72] D.W. Repperger, R.G. Roberts, C.G. Koepke, Quantitative measurements of system complexity, 2012, US Patent 8, 244, 503 B1.
[73] E. Jen, Robust Design: a Repertoire of Biological, Ecological, and Engineering Case Studies, Oxford University Press, ISBN: 9780195165333, 2005.
[74] D.G. Thomas, D.S. Bywaters, System stability and conclusions, in: The Creators of Inside Money, Springer, 2021, pp. 211–215, http://dx.doi.org/10.1007/978-3-030-70366-0_13.
[75] A. Xue, S. Mei, B. Xie, A comprehensive method to compute the controlling unstable equilibrium point, in: 2008 Third International Conference on Electric Utility Deregulation and Restructuring and Power Technologies, IEEE, 2008, pp. 1115–1120.
[76] L. Qiaoge, F. Mengyin, S. Changsheng, Study of the control-equilibrium of control systems, J. Syst. Eng. Electron. 19 (4) (2008) 775–778.
[77] L. Bai, W. Zhou, The measurement of transient stability with high resolution, in: 2013 Joint European Frequency and Time Forum & International Frequency Control Symposium, EFTF/IFC, IEEE, 2013, pp. 175–178.
[78] E. Yaz, Deterministic and stochastic robustness measures for discrete systems, IEEE Trans. Autom. Control 33 (10) (1988) 952–955.
[79] E. Yaz, X. Niu, New robustness bounds for discrete systems with random perturbations, IEEE Trans. Autom. Control 38 (12) (1993) 1866–1870.
[80] R. Klomp, C. Borst, R. van Paassen, M. Mulder, Expertise level, control strategies, and robustness in future air traffic control decision aiding, IEEE Trans. Hum.-Mach. Syst. 46 (2) (2016) 255–266.
[81] M.S. Phadke, Quality Engineering Using Robust Design, Prentice Hall PTR, 1989.
[82] D.G. Ullman, Making Robust Decisions: Decision Management for Technical, Business, and Service Teams, Trafford Victoria, Canada, 2006.
[83] R.J. Lempert, M.T. Collins, Managing the risk of uncertain threshold responses: comparison of robust, optimum, and precautionary approaches, Risk Anal.: An Int. J. 27 (4) (2007) 1009–1026.
[84] R.L.N.S. Schlesinger, Characterizing climate-change uncertainties for decision-makers. An editorial essay, Clim. Change 65 (1–2) (2004) 1.
[85] P. Croskerry, A universal model of diagnostic reasoning, Acad. Med. 84 (8) (2009) 1022–1028.
[86] J.C. Marshall, L. Bosco, N.K. Adhikari, B. Connolly, J.V. Diaz, T. Dorman, R.A. Fowler, G. Meyfroidt, S. Nakagawa, P. Pelosi, et al., What is an intensive care unit? A report of the task force of the world federation of societies of intensive and critical care medicine, J. Crit. Care 37 (2017) 270–276.
[87] W. Stallings, Computer Organization and Architecture: Designing for Performance, Pearson Education India, 2003.
[88] A.S. Tanenbaum, Structured Computer Organization, Pearson Education India, 2016.
[89] W.C. Lynch, Operating system performance, Commun. ACM 15 (7) (1972) 579–585.
[90] K.M. Sacha, Measuring the real-time operating system performance, in: Proceedings Seventh Euromicro Workshop on Real-Time Systems, IEEE, 1995, pp. 34–40.
[91] S.-T. Kung, C.-C. Cheng, C.-C. Liu, Y.-C. Chen, Dynamic power saving by monitoring CPU utilization, 2003, US Patent 6, 574, 739.
[92] E. Menezes, D.F. Tobias, R. Russell, M. Altmejd, CPU utilization measurement techniques for use in power management, 2005, US Patent 6, 845, 456.
[93] J.B. Chen, B.N. Bershad, The impact of operating system structure on memory system performance, in: Proceedings of the Fourteenth ACM Symposium on Operating Systems Principles, 1993, pp. 120–133.
[94] D. Kayande, U. Shrawankar, Performance analysis for improved RAM utilization, in: 2012 CSI Sixth International Conference on Software Engineering, CONSEG, IEEE, 2012, pp. 1–6.
[95] J.B. Page, Method for balancing the utilization of input/output devices, 1972, US Patent 3, 702, 006.
[96] C. Priem, D.S. Rosenthal, Architecture for providing input/output operations in a computer system, 1997, US Patent 5, 623, 692.
[97] R.H. Katz, G.A. Gibson, D.A. Patterson, Disk system architectures for high performance computing, Proc. IEEE 77 (12) (1989) 1842–1858.
[98] Y. Guo, B. McNutt, J. Tian, Y. Xu, Estimation of performance utilization of a storage device, 2019, US Patent 10, 209, 898.
[99] D.N. Cutler, C.T. Lenzmeier, Queue object for controlling concurrency in a computer system, 1998, US Patent 5, 752, 031.
[100] D.E. Bohm, R.G. LaBrie, D.E. Reyes, System and method for utilizing dispatch queues in a multiprocessor data processing system, 2004, US Patent 6, 834, 385.
[101] R. Pierre, Process for improving the performance of a multiprocessor system comprising a job queue and system architecture for implementing the process, 2006, US Patent 6, 993, 762.
[102] S.N.M. Shah, A.K.B. Mahmood, A. Oxley, Hybrid scheduling and dual queue scheduling, in: 2009 2nd IEEE International Conference on Computer Science and Information Technology, IEEE, 2009, pp. 539–543.
[103] J.D. Valladolid, J.S. Abril, A.D. Valdiviezo, Analysis of EnergyEfficient in traction and breaking for electric vehicles through laboratory experiments, in: Smart Innovation, Systems and Technologies, Springer Singapore, ISBN: 9789811641251, 2021, pp. 297–305, http://dx.doi.org/10.1007/978-981-16-4126-8_28.
[104] S. Kadam, T. Dhanadhya, D. Patil, S. Prasad, D. Kanase, Optimizing efficiency and extending battery life in electric vehicles: A comprehensive analysis of system components and design strategies, in: 2024 International Conference on Intelligent Systems and Advanced Applications, ICISAA, IEEE, 2024, pp. 1–6, http://dx.doi.org/10.1109/icisaa62385.2024.10829358.
[105] F.P. Carmona, J.J.R. Rivas, D.M. Garduño, O.C. Castillo, R.O. González, Simulation of a traction system in an electric vehicle, in: 2023 IEEE International Autumn Meeting on Power, Electronics and Computing, ROPEC, IEEE, 2023, pp. 1–6, http://dx.doi.org/10.1109/ropec58757.2023.10409447.
[106] D.P. S., C. P., C. C., S. A., B. F., M. G., P. P., On the comparison of 2- and 4-wheel-drive electric vehicle layouts with central motors and single- and 2-speed transmission systems, Energies (2020) http://dx.doi.org/10.3390/en13133328.
[107] Y. Sun, H. Xiong, Job-shop scheduling problem based on particle swarm optimization algorithm, Sens. Transducers 16 (2012) 116.
[108] M. Safdari, R. Ahmadi, S. Sadeghzadeh, Numerical and experimental investigation on electric vehicles battery thermal management under new European driving cycle, Appl. Energy 315 (2022) 119026.
[109] S. Kang, K. Min, Dynamic simulation of a fuel cell hybrid vehicle during the federal test procedure-75 driving cycle, Appl. Energy 161 (2016) 181–196.
[110] ISO, Standard Atmosphere, ISO 2533:1975 ed., International Organization for Standardization, 1975.
[111] M. Ehsani, Y. Gao, S. Longo, K.M. Ebrahimi, Modern Electric, Hybrid Electric, and Fuel Cell Vehicles, CRC Press, 2018.
[112] E. Bartholomew, J.H. Kwakkel, On considering robustness in the search phase of robust decision making: A comparison of many-objective robust decision making, multi-scenario many-objective robust decision making, and many objective robust optimization, Environ. Model. Softw. 127 (2020) 104699.
[113] C. McPhail, H. Maier, S. Westra, J. Kwakkel, L. Van Der Linden, Impact of scenario selection on robustness, Water Resour. Res. 56 (9) (2020) e2019WR026515.
[114] S. Homaei, M. Hamdy, A robustness-based decision making approach for multi-target high performance buildings under uncertain scenarios, Appl. Energy 267 (2020) 114868.

João Ricardo Braga de Paiva: He holds a Dr. and M.Sc. in Electrical and Computer Engineering from the Federal University of Goias. He is a Professor at the Federal Institute of Goias and a member of the GCITE research group. His research focuses on the modeling, simulation, and optimization of discrete event systems, particularly in metrics of performance, complexity, stability, and robustness.

Viviane Margarida Gomes Pacheco: Holds a Doctorate in Systems Complexity from the Federal University of Goiás, with a research exchange at Carleton University, Canada. Currently, she coordinates teaching, research, and extension activities at the Federal Institute of Goiás. Her expertise includes innovation, intellectual property, system complexity, and computational intelligence.

Júnio Santos Bulhoes: Holds a Dr. in control systems applied from the Federal University of Goiás (2024) and a M.Sc. in system identification. He is a Professor at the Federal Institute of Mato Grosso with research focusing on control systems and automation.

Clóves Gonçalves Rodrigues: Dr. in Physics from UNICAMP, where he also completed a postdoctoral fellowship. He is a full professor at PUC-GO and collaborates with the Joint Institute for Nuclear Research in Moscow. His research interests lie in production engineering and systems.

António Paulo Mendes Breda Dias Coimbra: Holds a Dr. in Electrical Engineering from the University of Coimbra. He is an Assistant Professor at the University of Coimbra and a researcher at the Institute of Systems and Robotics. His research focuses on biped robots, hyper-redundant robots, and electromagnetic compatibility.

Wesley Pacheco Calixto: Dr. in Electrical Engineering from the Federal University of Uberlândia, with a research period at the University of Coimbra. He is a Professor at the Federal Institute of Goias with research focusing on system modeling, intelligent systems, and process optimization.